U.S.NRC
United States Nuclear Regulatory Commission
Protecting People and the Environment

Technical Letter Report

TLR-RES/DE/CIB-2021-01

Estimation Scheme for Weld Residual Stress Effect on Crack Opening Displacements

Date:

September 18, 2020

Prepared in response to Task 3 in User Need Request NRR-2020-004, by:

F.W. Brust
Engineering Mechanics Corporation of Columbus

E. Punch
Engineering Mechanics Corporation of Columbus

E. Twombly
Engineering Mechanics Corporation of Columbus

NRC Project Manager:

Jay Wallace
Materials Engineer
Component Integrity Branch

Division of Engineering
Office of Nuclear Regulatory Research
U.S. Nuclear Regulatory Commission
Washington, DC 20555–0001

DISCLAIMER

This report does not contain or imply legally binding requirements. Nor does this report establish or modify any regulatory guidance or positions of the U.S. Nuclear Regulatory Commission and is not binding on the Commission.

Final Report On

Estimation Scheme for Weld Residual Stress Effect on Crack Opening Displacements

U.S. Nuclear Regulatory Commission
Prime Contract No.: NRC-HQ-25-14-E-0004
NUMARK Job No. 4409, Task Order 9
Emc^2 Project Number: 17-G121-01

As a Subcontractor to NUMARK Associates, Inc.
to

U.S. Nuclear Regulatory Commission
Washington, D.C. 20555-0001
by

F.W. Brust, E. Punch, E. Twombly

Engineering Mechanics Corporation of Columbus
3518 Riverside Drive, Suite 202
Columbus, OH 43221
Phone/Fax (614) 459-3200/6800

September 18, 2020

As a Subcontractor to
NUMARK Associates, Inc.
1220 19th Street, NW, Suite 500
Washington, DC 20036

Executive Summary

Evaluating leak before break (LBB) in nuclear piping systems requires determination of leak rate which critically depends on crack opening displacement (COD). Procedures have been developed for accurately estimating the COD resulting from service loads in pipes. However, cracks in nuclear piping and nozzles often occur in and near welds, and the weld residual stresses (WRS) can strongly affect the COD values. Although WRS-influenced COD changes can in some cases close and stop leakage, thus hinder leak detection, the effects have been typically neglected because they could only be evaluated on a case-by-case basis using finite element calculations.

This report presents a simple estimation scheme that was developed along the lines of classical COD estimation schemes that use influence functions developed from finite element solutions. This estimation scheme has been validated for different WRS fields, a wide range of pipe sizes and for a wide range of crack sizes. The estimation scheme, its development and use, and the validation results are presented here.

ACKNOWLEDGEMENTS

The authors gratefully acknowledge the helpful comments provided by the NRC staff during the preparation of this report. In particular, the extensive comments, edits, and contributions from the Office of Nuclear Reactor Regulation and the Component Integrity Branch are gratefully appreciated.

Estimation Scheme for Weld Residual Stress Effect on Crack Opening Displacements

F.W. Brust, E. Punch, E. Twombly

1. Introduction

Leak before Break (LBB) concepts have been used in many industries (nuclear, space, oil, and gas, etc.) over the years to help ensure that pressurized pipes, vessels, and other components operate safely. With LBB a pressurized component will leak, and the leak must be detected so that the component can be depressurized, and the flaw repaired, or pipe or vessel replaced before a catastrophic break occurs. The nuclear industry has been one of the leaders in LBB technology development over the years. LBB is used in nuclear plants to simplify the plant design to ensure jet impingement shields, pipe whip constraints, and other safety features are not required.

The Standard Review Plan in NUREG-0800 was developed by the U.S. Nuclear Regulatory Commission and provides LBB evaluation procedures to exclude the dynamic effects of postulated pipe ruptures. In particular, the Standard Review Plan (SRP) Section 3.6.3 allows analyses to eliminate postulated pipe ruptures from the design basis of plant SSCs. Part of this analysis plan is to determine the leak rate through postulated cracks that are smaller than the critical size with safety factors applied on both loads and crack size. The leak rate codes require inputs of the crack length and the crack opening displacement (COD), the separation or opening between crack faces, to predict the leak rate.

Analytical methods for estimating COD from operating loads have been developed to eliminate the necessity of performing finite element (FE) solutions for each individual geometry and loading condition on a case by case basis. However, cracks in piping often occur in welds or in the heat affected zone of welds, and weld residual stresses can also affect the COD. The effect of the WRS and COD is usually ignored in LBB calculations mainly because no adequate estimation method has been available to predict this effect to date. This report examines various analytical methodologies for estimating WRS-induced COD and provides an estimation scheme similar to the classic GE/EPRI method (Kumar et al, 1980) that can be used to predict the effect of WRS on COD.

Validation examples are provided where COD estimates are compared directly to full WRS solutions with a crack added, for a large number of cases. This is followed by a summary of the results and suggestions for possible additional work.

2. Preliminary Work on WRS / COD Evaluation

During this work several methods were investigated in order to develop a simple engineering estimation method that would be adequate for predicting the effect of WRS on COD. We only provide a short summary of the methods attempted here; further discussion is provided in the program monthly reports over the program duration.

One method that was examined was a 'crack plate analogy', an appealing method because the result of the method was a simple equation. WRS effects on COD were evaluated using a plate theory analogy that used the effective moment from the axis-symmetric WRS fields and applied it to a plate as a boundary traction which is meant to represent the crack face of the through-wall cracked pipe (Olson, 2016). A series of plate element finite element solutions was performed as part of this work and these were compared to the crack-plate analogy theory COD predictions. The results of the comparison showed that plate theory does not apply to thick DMW welded pipe because typical small R_m/t renders plate theory invalid. This method, however, may have promise for thin pipe.

A second simple method was examined based on COD predictions from the LBB.ENG elastic-plastic fracture method (Brust et al, 1993). The LBB.ENG methods (there are several related methods including one for welded pipe) provide excellent predictions of J-integral for through-wall cracks. However, the method used to predict COD was found to not be sufficiently accurate, so this method was abandoned.

For this work axis-symmetric FE calculations were performed for a wide range of R_m/t values and crack sizes in order to develop a database of pipe geometry – crack length - COD solutions. The axial WRS field obtained from axis-symmetric FE solution is inherently self-equilibrated, suggesting that a crack face moment load analogy could be employed in developing a predictive method. Therefore, an estimation scheme similar to the classic GE/EPRI method (Kumar et al, 1980) was developed with a series of V_{1WRS} influence functions for a 'unit' moment to the pipe crack face. This method assumes that the effect of WRS on COD is dominated by the elastic response which, as will be shown, is a good assumption. To apply the method, one uses GE/EPRI-like V_{1WRS} influence functions along with the actual WRS field from weld analyses to estimate the COD caused by the WRS field.

3. Development of GE/EPRI-like WRS / COD Influence Function

In order to generate data for input into GE/EPRI-like V_{1WRS} determinations, finite element-based predictions of COD were performed. FE calculations have shown that the form of the stress field (linear, parabolic, etc.) does not greatly affect the COD compared to the moment produced from the actual WRS field. Therefore, a linear stress field was chosen to evaluate crack face moments and COD to develop V_{1WRS} influence functions. Since the WRS field obtained from axis-symmetric FE solution was inherently self-equilibrated, axial tension forces were not considered. Also, plastic effects were not considered.

3.1 Overview of GE/EPRI-Like COD Estimation Method

Estimation schemes were developed by the NRC over the years to predict crack instability and crack opening displacements. The validity of estimation schemes to characterize both instability and crack opening is based on J-Tearing theory which was originally developed by Rice and Rosengren (1968) and Hutchinson (1968). This effort focuses on COD estimation, but the general J-Tearing theory and classical J-estimation methods and theory that are used for crack stability and COD estimates by the US NRC are briefly reviewed in Appendix A for completeness.

COD estimation methods for forces and moments applied to a pipe were originally developed by Kumar et al. (1981, 1984, 1988) and were improved for small through-wall cracks by the NRC (Brust, 1995). Young et al (2012, 2013) recently improved on the legacy COD estimation schemes by using updated finite element models. These solutions are currently used within the xLPR code. With this method

influence functions are calculated for both the elastic and fully plastic COD. These are then added together to obtain the total COD. The influence functions of Young are compiled for various mid-radius over thickness (R_m/t) ratios, different crack sizes, different loading conditions (axial tension, bending, and crack face pressure) and for various Ramberg-Osgood hardening coefficients, as summarized by Young et al (2012, 2013).

The form for the elastic COD from Young (2012, 2013) for pipe is shown in Equation (1).

$$\delta^{el} = \frac{4a}{E}\sigma_c V_{1c}\left(\frac{\theta}{\pi}, \frac{R_m}{t}\right) \qquad (1)$$

where δ^{el} is the elastic COD, a is crack size (total crack size = 2a), E is elastic modulus, σ_c is load component converted to appropriate stress, V_{1c} is the numerically calculated influence function, θ is half crack angle, R_m is mean radius, and t is thickness. Young (2012) compiled separate influence functions for each category of load (σ_c), axial tension (caused by end cap pressure and/or applied axial tension), bending stress, and crack face pressure. The V_1 functions are tabulated for the various load conditions at the pipe ID, mid wall thickness (MW), and OD so that COD of the cracked pipe can be determined.

For the plastic solution contributions, similar influence functions are tabulated for various values of the Ramberg-Osgood hardening exponent (n) and these are not written out here (see Young (2012)). These influence functions are called h_2 and are consistent with the original definitions of Kumar (1988). The COD from service loads is then calculated by adding the three elastic and three plastic components together. In practice for service loads the elastic COD solutions dominate for smaller cracks and plastic contributions will not be considered here.

3.2 Crack Face Moment for a Linear Stress Field

As noted in the overview of the GE/EPRI-like estimation method, the influence function is dependent on the crack size (θ/π), pipe geometry (R_m/t) and the load category (tension or bending). Axis-symmetric FE calculations imply that WRS crack face tractions can be represented as a crack face moment without any axial component. Therefore, only the bending moment influence functions are evaluated here as caused by the WRS field. To develop the V_{1WRS} functions which are used to estimate the effect of COD from the WRS field, a linear WRS field from -100 MPa at the inside diameter (ID) to +100 MPa at the outside diameter (OD) was applied to the cracked pipe with the correction for disequilibrium applied as discussed below.

It can be shown (see Appendix B) that the moment for this linear stress field is given by the expression:

$$M = \frac{\sigma_{nom} t^2 \left[1 - \frac{1}{12\left(\frac{R_m}{t}\right)^2}\right]}{6} \qquad (2)$$

For a nominal stress field of +- 100 MPa, this moment is 6236.71 for the pipe size given in Table 4 (below) and this moment changes depending on the R_m/t of the pipe. However, when using the nominal linear stress field to develop the V_{1WRS} functions, the nominal WRS field must be in equilibrium which is

not achieved here because a pipe has curvature, i.e., larger OD circumference than ID circumference. The correction on the stress field to ensure equilibrium can be shown to be (Appendix B):

$$\sigma_{dis} = \frac{\sigma_{nom}}{6\left(\frac{R_m}{t}\right)} \qquad (3)$$

This results in σ_{dis}=1.67 MPa for the nominal stress field for this size pipe. Therefore, when developing the V_{1WRS} functions (below) a stress field of -101.67 and +98.33 MPa are applied at the ID and OD with linear distribution between.

3.3 Development of WRS Influence Functions

A total of 96 meshes were developed for FE calculations of COD that were used to develop V_{1WRS} influence functions. Finite element meshes were developed with refined meshes with cracks inserted (for example meshes please see Appendix C for examples). There are three dimensional meshes and the axis-symmetric type moments with nominal stresses (+- 100 MPa) were applied along the crack for each crack size and geometry. The calculations were performed using a +- 100 MPa moment load (with adjustments to render the stresses self-equilibrated as per equation (3)) for a wide range of crack sizes ($0.00556 <= \theta/\pi <= 0.3333$) and pipe geometries ($2 <= Rm/t <= 20$). (Further details of the FE procedure are provided in Appendix C.)

These data were then incorporated in a GE/EPRI-like estimation method for determining the V_{1WRS} influence functions. In addition, numerous additional meshes and analyses were developed to ensure that the mesh refinement was sufficient to ensure convergence of the V_{1WRS} influence functions. Table 1 through Table 3 provide V_{1WRS} for four R_m/t values (2, 5, 10, 20) and eight half-crack angles (1°, 2.5°, 5°, 10°, 22.5°, 33.75°, 45°, 60°). In the tables the crack angles are listed as θ/π = (0.00556, 0.01389, 0.02780, 0.05556, 0.125, 0.1875, 0.25, 0.333) rather than as angles although they are equivalent. Analyses were also made for R_m/t = 3.5 and 7.5 and these values are compared to linear interpolation within Table 1 through Table 3 for validation although not summarized in this report. This comparison showed that linear interpolation produced acceptable results.

FE calculations for crack angles greater than 60-degrees were not performed because the effect of WRS for larger cracks sizes can be ignored because service load CODs dominate.

The COD estimate for WRS effect can be written as:

$$\delta_{WRS}^{el} = \frac{4a}{E}\sigma_{WRS}V_{1WRS}\left(\frac{\theta}{\pi}, \frac{R_m}{t}\right) \qquad (4)$$

The values of the influence functions in Tables 1 through 3 were calculated by rearranging Eq. 4 and solving for V_{1WRS}.using the FE COD determinations for each crack size and Rm/t value at the ID, MW and OD.

Table 1 V_{1WRS} for ID

θ/π R_m/t	0.0056	0.0139	0.0278	0.0556	0.1250	0.1875	0.2500	0.3333
20	-0.7963	-0.5997	-0.4617	-0.3237	-0.1507	-0.0863	-0.0532	-0.0297
10	-0.8965	-0.7320	-0.5739	-0.4144	-0.2184	-0.1254	-0.0652	-0.0114
5	-0.9289	-0.8301	-0.6992	-0.5279	-0.3050	-0.1894	-0.1050	-0.0174
2	-0.8354	-0.8077	-0.7584	-0.6589	-0.4461	-0.3049	-0.1883	-0.0482

Table 2 V_{1WRS} for MW

θ/π R_m/t	0.0056	0.0139	0.0278	0.0556	0.1250	0.1875	0.2500	0.3333
20	0.0083	0.0167	0.0293	0.0498	0.0662	0.0595	0.0535	0.0480
10	0.0082	0.0193	0.0312	0.0506	0.0805	0.0898	0.0980	0.1092
5	0.0062	0.0209	0.0375	0.0580	0.0941	0.1152	0.1380	0.1707
2	0.0030	0.0159	0.0412	0.0798	0.1343	0.1705	0.2167	0.2915

Table 3 V_{1WRS} for OD

θ/π R_m/t	0.0056	0.0139	0.0278	0.0556	0.1250	0.1875	0.2500	0.3333
20	0.8249	0.6333	0.5184	0.4213	0.2817	0.2045	0.1594	0.1252
10	0.9667	0.7861	0.6365	0.5119	0.3763	0.3024	0.2593	0.2283
5	1.1017	0.9587	0.8050	0.6447	0.4866	0.4141	0.3761	0.3550
2	1.3506	1.2450	1.1131	0.9381	0.7258	0.6397	0.6115	0.6211

The definition of the weld residual stress (WRS) stress (σ_{WRS}) and the corresponding WRS moment to use for the equations is described in the next section.

4. Crack Face Moment for an Arbitrary Stress Field

This section introduces the crack face moment calculation for circumferential TWC cracks in non-stress-relieved nozzle welds. This is the moment produced by the effect of the WRS field affecting the COD values. The axial WRS field is obtained from an axis-symmetric FE solution and is, therefore, self-equilibrated, suggesting that it can be represented by a moment load analogy presented in the previous section. This pure moment induces stresses of opposite sign throughout the thickness and is often compressive on the ID for thick DMW pipe welds. It should be noted that the present WRS/COD estimation scheme will not be valid for full three-dimensional WRS fields produced using virtual fabrication technology (VFT) where start/stop effects render the WRS field non axis symmetric.

While an arbitrary WRS field is not, in general, linear through the wall thickness, the crack face moment for an arbitrary WRS field can be approximated. It is important to note that the definition of moment is somewhat arbitrary, and the WRS/COD estimation scheme will be valid only when using this consistent definition of the moment induced by the WRS field. Since the WRS field is assumed to be axis-symmetric, one only need define a moment per unit arc length or angle. We could define the moment on a 1-degree arc or other angular arc, but we choose to define the angle by a unit arc length, 1 mm, at the mid thickness of the cylinder. This angle is such that arc length is $R_m*\theta = 1$, or $\theta = 1/R_m$, where R_m is the mean radius in mm and θ is the angle in radians. The WRS field and crack face moment is then defined over this angle.

For the example shown here, FE calculations were employed to determine the WRS field and COD resulting from welding for a $R_m/t=10$ pipe geometry (Table 4). Details of the FE procedure can be found in Appendix C. The calculated WRS field is given in the blue curve in Figure 1 and the WRS field values are tabulated through the thickness in the WRS axial component column of

Table **5**. Please keep in mind that the example provided below, which defines how to obtain the WRS moment, and therefore the σ_{WRS} field to use in estimating the effect of WRS COD using equation 4, depends on both the geometry and WRS field. In Figure 1 the term 'two part' WRS field is defined in Appendix C. This term is used because the thermal gradient field used to mimic the WRS field requires two separate thermal field definitions through the pipe wall to obtain the WRS field (see Figure 18 in Appendix C for the 'one part' WRS definition). These are both used in the validation section provided next to illustrate that the WRS COD estimation scheme is valid for arbitrary WRS fields through the thickness.

Table 4 Example pipe geometry for crack face moment calculation example

Outside diameter	**406.4 mm**
Wall thickness T	**19.3524**
Elastic Modulus	**200,000 MPa**
Rm / t	**10**

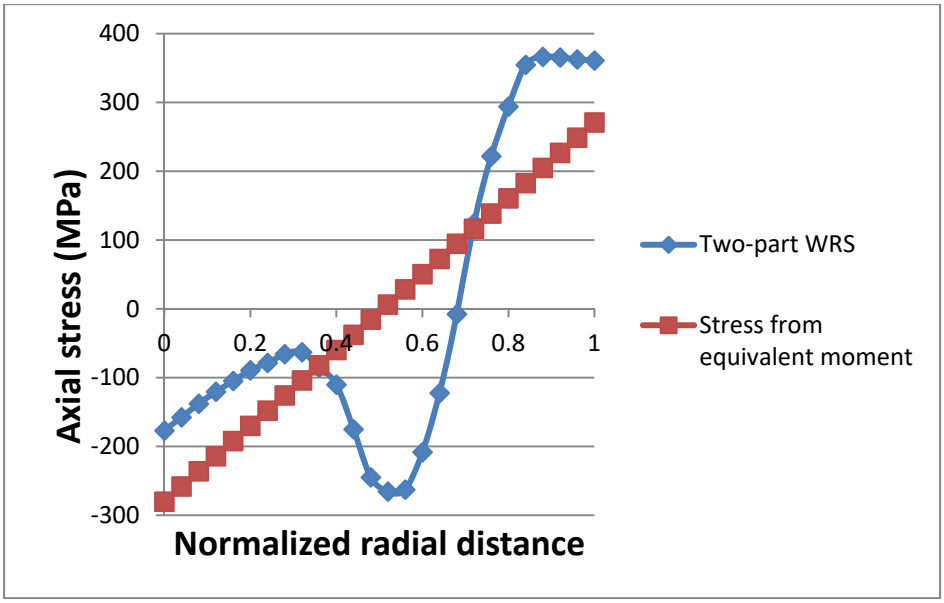

Figure 1 WRS distribution through the pipe thickness for example moment calculation

It has been found that an arbitrary WRS field can be well-described with 26 equidistant points (25 segments or a larger number of segments) as a function of radial position through the pipe wall thickness. Figure 2 illustrates the mean radius of each of the segments for the arc length θ. The segment radial dimension is t/25 here and the intervals of distance from the inside diameter, x, over thickness, t, are x/t = 0.04 for this case (i.e., x/t = 0, 0.04, 0.08, …, 0.96, 1.0). If we take the average stress in each of

the 25 segments and multiply by the area of each segment[1], we obtain the incremental force in each segment.

For WRS fields obtained from axis symmetric finite element weld analysis, summing the forces through the thickness should result in only a very small value of dis-equilibrium that is the due to numerical error.

If we take each incremental force multiplied by the radial distance from the pipe center to the center of the segment we obtain the incremental moment about the center of the pipe wall thickness, which when summed through the thickness provides the crack face moment caused by the WRS field. It is this moment, normalized by the thickness squared divided by 6 (to obtain a WRS 'stress'), that is used in the COD estimation scheme. Once the WRS moment is calculated, the WRS stress is evaluated using Equation 6 (below) and this is the value used to calculate the WRS COD from Equation 4 using the appropriate values of V_{1WRS}. For the pipe geometry example here (Table 4) these values are shown in

[1] The area of each segment can be estimated by taking the radius (R) to the center of the segment times the angle ($\theta=1/R_m$) times the segment depth (0.04t here), or area of each segment is (R/Rm)(0.04t).

Table **5**.

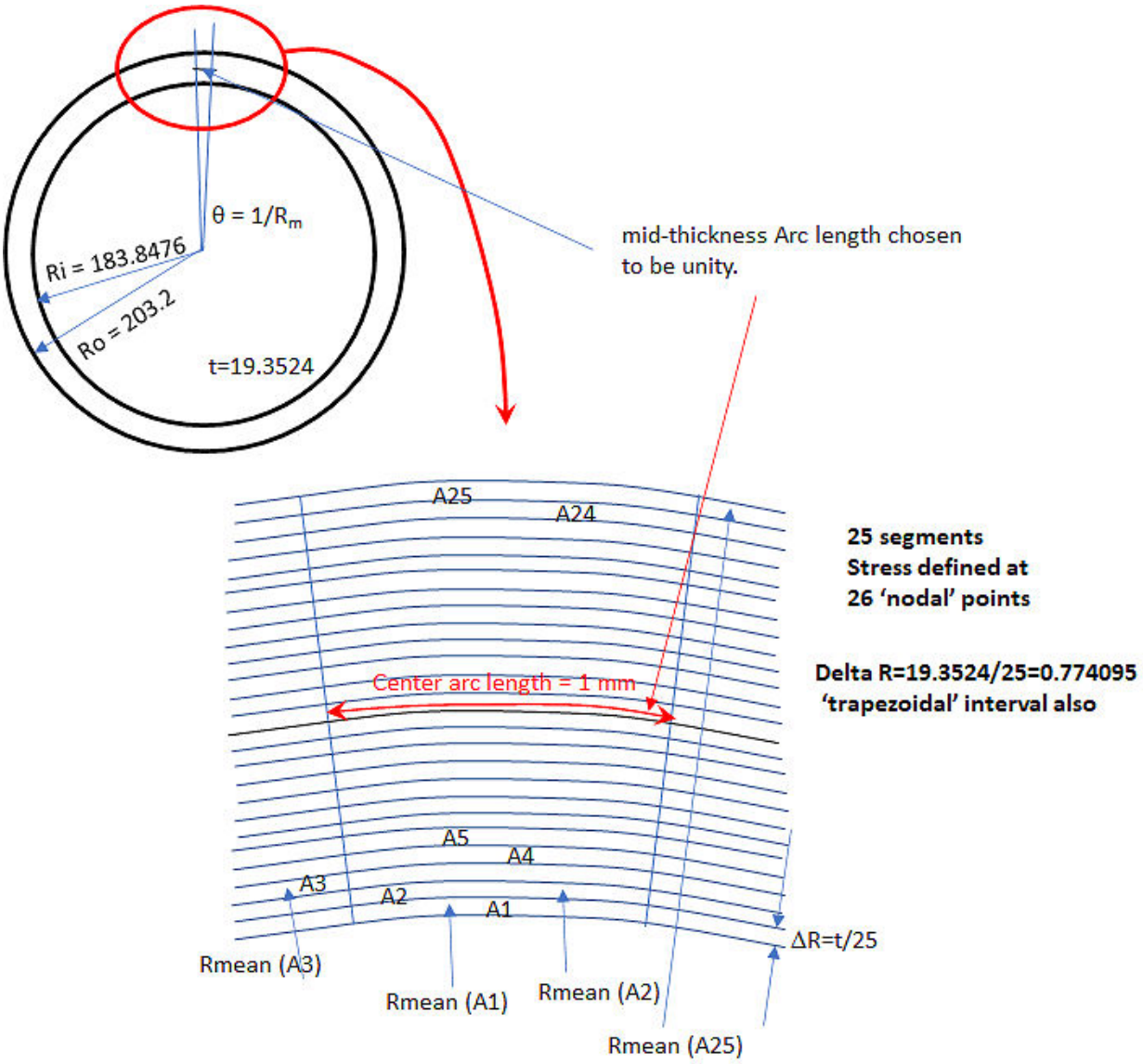

Figure 2 Sector of pipe and increments for integration by trapezoidal rule

Table 5 Incremental and total WRS axial force and moment by trapezoidal rule

x/t	Segment Arc length (mm)	Trapezoid weight* increment (mm)	Lever arm about pipe center line (mm)	WRS axial component (MPa)	Inc.axial force= WRS*length * weight (N)	Inc.moment= Force*Lever (N-mm)
0	0.95	0.3870475	183.8476	-176.84	-65.0232	-11954.4
0.04	0.954	0.774095	184.6217	-157.573	-116.366	-21483.6
0.08	0.958	0.774095	185.3958	-137.953	-102.304	-18966.7
0.12	0.962	0.774095	186.1699	-120.44	-89.6892	-16697.4
0.16	0.966	0.774095	186.944	-104.825	-78.3856	-14653.7
0.2	0.97	0.774095	187.7181	-89.2528	-67.0175	-12580.4
0.24	0.974	0.774095	188.4922	-78.5322	-59.2108	-11160.8
0.28	0.978	0.774095	189.2663	-65.7475	-49.7751	-9420.76
0.32	0.982	0.774095	190.0404	-62.8895	-47.8062	-9085.1
0.36	0.986	0.774095	190.8145	-85.2274	-65.0505	-12412.6
0.4	0.99	0.774095	191.5886	-110.166	-84.4262	-16175.1
0.44	0.994	0.774095	192.3627	-175.097	-134.729	-25916.7
0.48	0.998	0.774095	193.1368	-244.844	-189.154	-36532.5
0.52	1.002	0.774095	193.9109	-265.478	-205.916	-39929.4
0.56	1.006	0.774095	194.685	-262.891	-204.724	-39856.6
0.6	1.01	0.774095	195.459	-208.336	-162.885	-31837.3
0.64	1.014	0.774095	196.2331	-122.271	-95.9745	-18833.4
0.68	1.018	0.774095	197.0072	-7.65472	-6.03214	-1188.38
0.72	1.022	0.774095	197.7813	124.249	98.29653	19441.22
0.76	1.026	0.774095	198.5554	221.886	176.2267	34990.76
0.8	1.03	0.774095	199.3295	294.013	234.4219	46727.2
0.84	1.034	0.774095	200.1036	354.829	284.0103	56831.48
0.88	1.038	0.774095	200.8777	366.41	294.4144	59141.29
0.92	1.042	0.774095	201.6518	365.519	294.8303	59453.06
0.96	1.046	0.774095	202.4259	362.809	293.7678	59466.2
1	1.05	0.3870475	203.2	361.157	146.7742	29824.52
					-1.72477 (N) **Sum of Axial force per unit arc length on mid-thickness**	**17190.97 (N-mm)** **Total Moment per unit arc length on mid-thickness**

As seen in

Table **5**, there are 26 equidistant points and 25 increments. Incremental WRS axial force & moment are calculated for each segment (columns 6 and 7) and then integrated by Simpson's trapezoidal rule to give the total force and moment. Trapezoidal weight is the radial distance of each segment (these are half at ID and OD) and arc length is the arc distance of each segment so the product of weight and arc length is segment area. Multiply area by stress and this is incremental force in each segment (column 6). Finally, incremental moment (column 7) is force multiplied by radial distance from pipe center. It is apparent that the WRS distribution is equilibrated (i.e. negligible total axial force -1.72477 N per unit arc length on mid-thickness). The disequilibrium stress is then approximated by this value divided by the thickness squared or σ_{dis} equal to 0.0046 MPa, which is negligible. The total crack face moment is 17190.97 N-mm (bottom of column 7).

5. WRS COD Estimation using V_{1WRS} Function List

We can rearrange Equation 4 and solve for the nominal linear stress field that is described by the moment that approximates the nonlinear WRS field:

$$\sigma_{nom} = \frac{6M_{WRS}}{t^2\left[1 - \frac{1}{12\left(\frac{R_m}{t}\right)^2}\right]} \qquad (5)$$

It should be noted that the maximum value for R_m/t term in the denominator is small, ≈ 2%, for the worst-case $R_m/t = 2$ considered here. Therefore, a simplified calculation of the linearized WRS field, σ_{WRS} can be written:

$$\sigma_{WRS} = \frac{6M_{WRS}}{t^2} \qquad (6)$$

The procedure to estimate the COD caused by an arbitrary residual stress field is then as follows: One calculates the moment caused by the residual stress field (M_{WRS}) using the procedure discussed above and the σ_{WRS} is calculated from Equation (6). The V_{1WRS} values for the ID, MW and OD are determined by interpolating within Table 1 through Table 3 as appropriate for crack size and R_m/t. Finally, the COD is estimated using Equation (4).

If the moment is such that the WRS field will close the crack at the ID then the values of the V_{1WRS} functions, as shown in the Table 1 through Table 3, are used as is. If the moment is the opposite, then all V_{1WRS} values are reversed in sign from what is in Table 1 through Table 3.

An example calculation is given here. Using the geometry parameters from Table 4 (t = 19.3524, R_m/t = 10) and the crack face moment from

Table **5** (M = 17,190.97) the σ_{wrs} is 275.383 MPa. Assuming a crack size of $\theta/\pi = 0.125$ (22.5°), a = 75.997 mm at the mid thickness, and from Table 1 to Table 3 the influence function values, V_{1WRS}, for $R_m/t = 10$ for the ID, mid wall (MW) and OD are -0.2184, 0.0805, and 0.3763, respectively. Inserting these values in Equation 4 yields the WRS contribution to total COD:

δ_{WRS} (ID) = -0.0914 mm

δ_{WRS} (MW) = 0.0337 mm

δ_{WRS} (OD) = 0.1575 mm

6. Validation Cases

The validity of the crack face moment methodology for estimating COD was evaluated by comparing the COD estimates to FE determinations for a range of pipe sizes (R_m/t values of 2, 5, 10, and 20) and crack lengths (θ/π values of 00556, 0.01389, 0.0278, 0.05556, 0.125, 0.1875, 0.25 and 0.3333). In addition, two different WRS fields were chosen: The One-Part and Two-Part WRS field discussed in Appendix C.

The crack face moment was calculated for each WRS field and for each geometry, and the $V1_{WRS}$ influence functions from Table 1 through Table 3 were then used to estimate the COD. These values were compared to the finite element COD solutions discussed in Appendix C. In addition to these synthetic cases, the COD estimates for a surge line ($R_m/t = 4.5$) and for an RPV hot leg geometry ($R_m/t = 6$) were also evaluated.

Predictions for these cases compared to finite element solution are shown in Figure 3 through Figure 10. Each data point in the plots in Figure 3 through Figure 10 represents a full finite element solution where the WRS field was introduced via thermal field which is different for each R_m/t value. These WRS fields varied for each pipe size considered (see Figure 21 in Appendix C to observe these differences). In these figures, the label 'COD by V1 designation' represents the prediction using the estimation scheme and 'COD by FEM' represents the full 3D finite element solutions. The 'ID, mid, and OD' represent inner, mid-wall, and outer diameter locations. The WRS moments are listed in the figure captions as well. It is seen that reasonable engineering estimates of the WRS COD fields are provided. Note that the WRS distributions for the One-Part and Two-Part fields (See Figure 18 and Figure 19 for the plots in Appendix C) produce similar COD values from the finite element results indicating that the linear stress fields used to obtain the V_{1WRS} functions is a reasonable engineering approach.

The estimation scheme provides good engineering estimates of the COD at the ID and OD of the pipes. The mid wall COD value predictions are less accurate for $R_m/t=2$ case in particular. The summary section provides a discussion of how to possibly improve the mid wall predictions for small R_m/t.

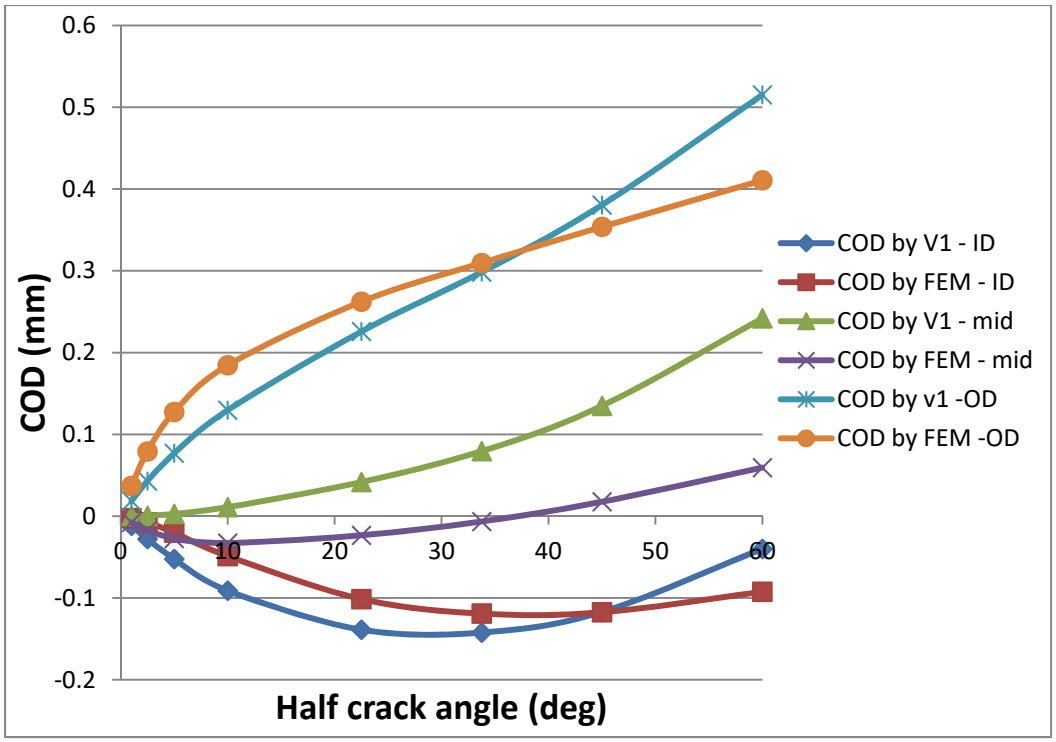

Figure 3 Validation of COD for One-Part WRS field (R_m/t=2; WRS Mom. = 268229.5 N-mm)

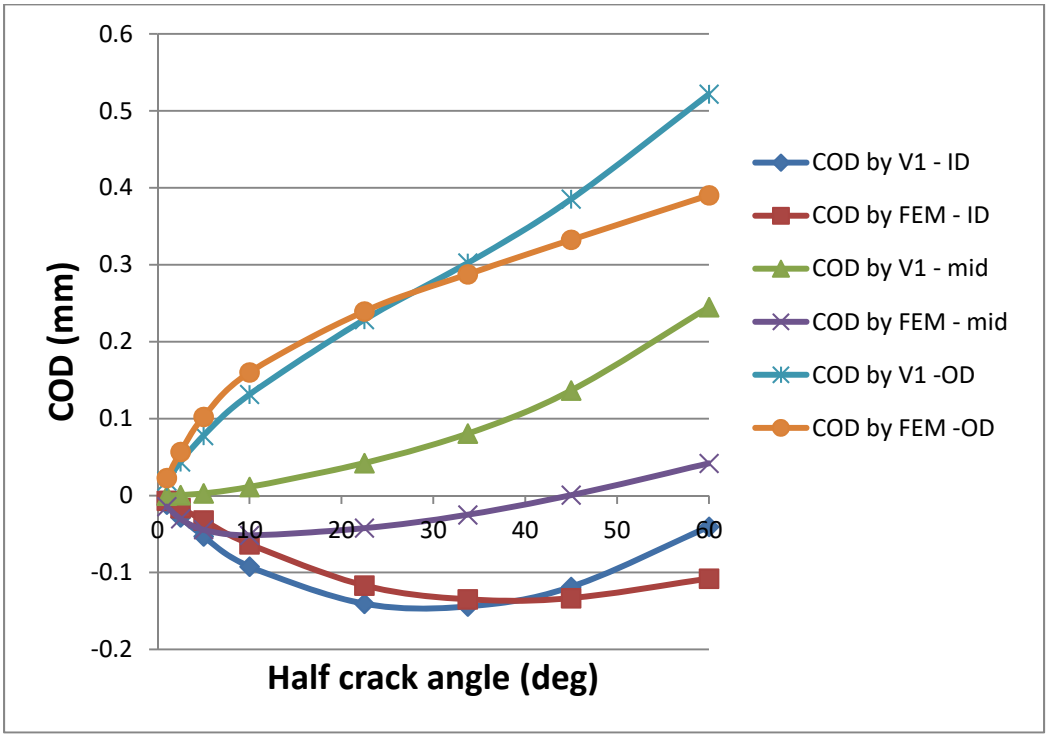

Figure 4 Validation of COD for Two-Part WRS field (R_m/t=2; WRS Mom. = 271710.8 N-mm)

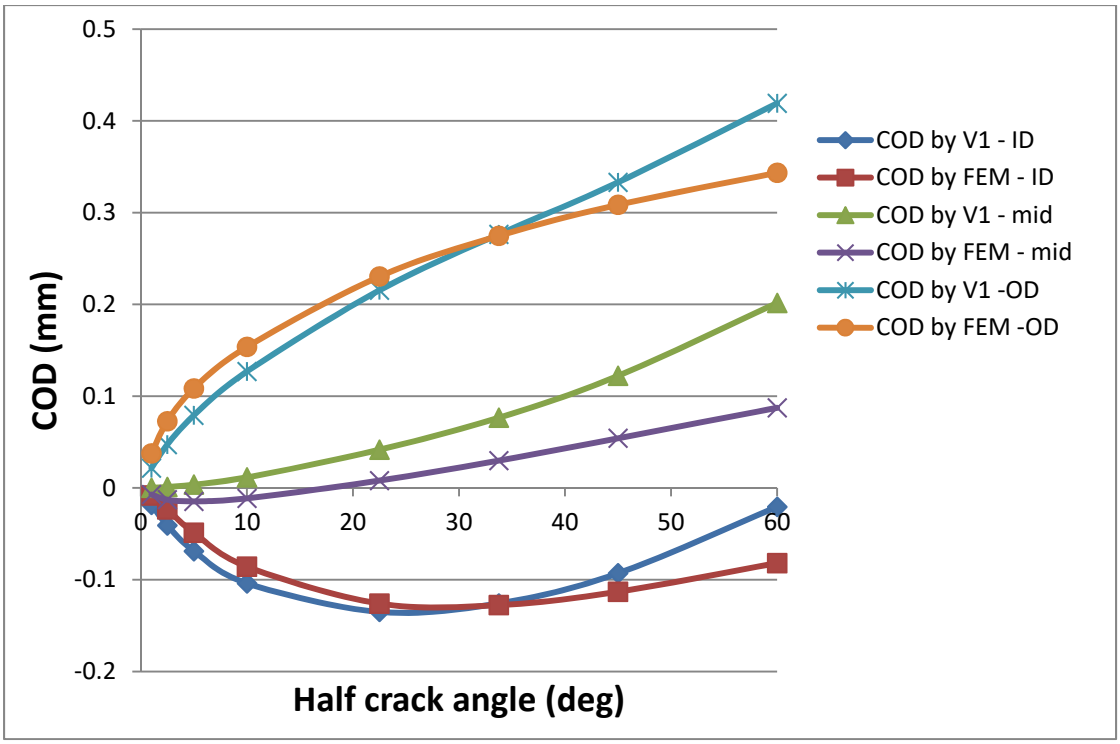

Figure 5 Validation of COD for One-Part WRS field (R_m/t=5; WRS Mom. = 69424.2 N-mm)

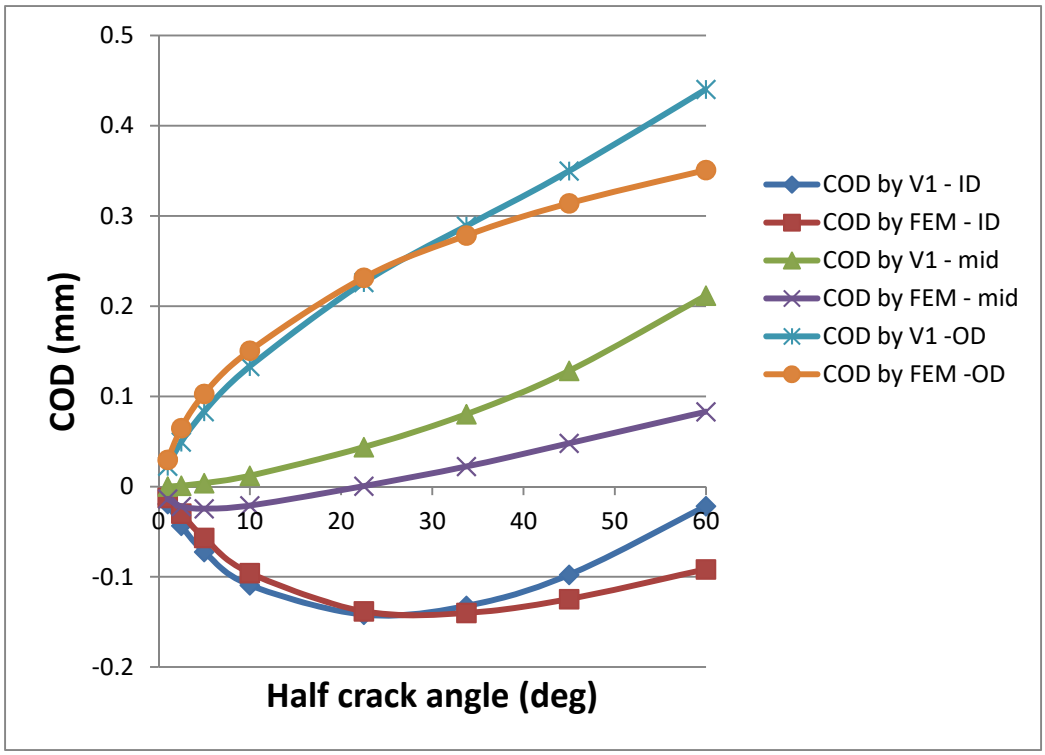

Figure 6 Validation of COD for Two-Part WRS field (R_m/t=5; WRS Mom. = 72945.1 N-mm)

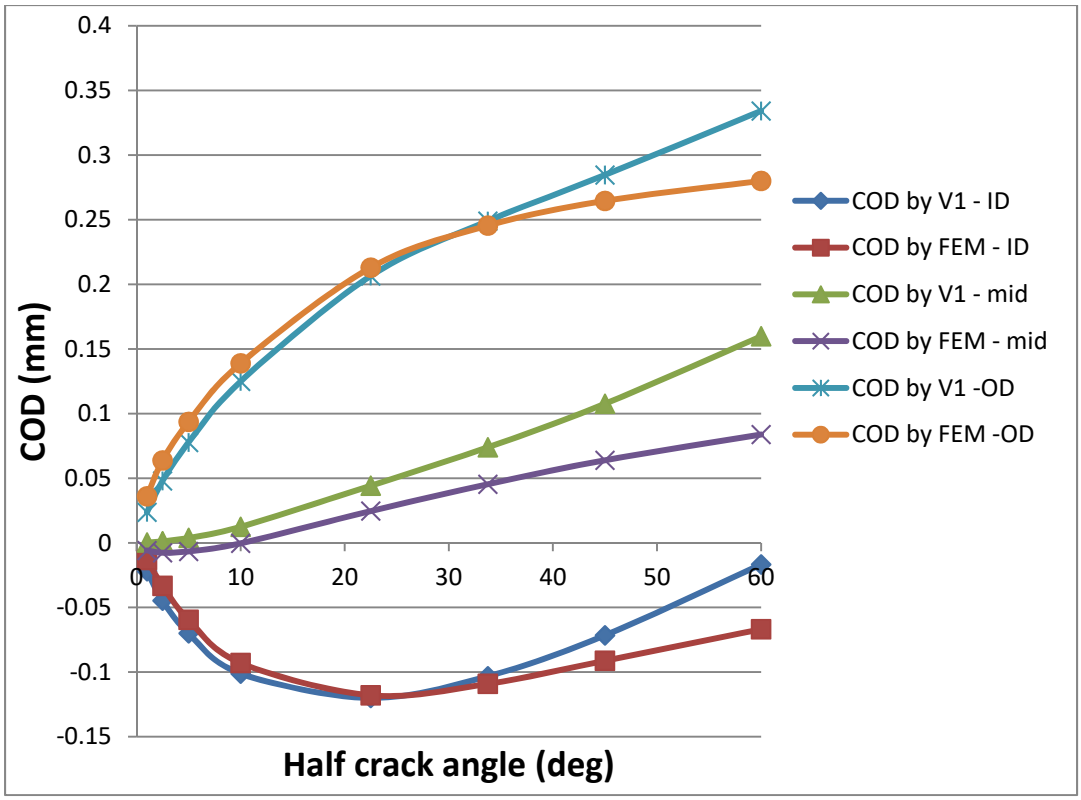

Figure 7 Validation of COD for One-Part WRS field (R_m/t=10; WRS Mom. = 22540.5 N-mm)

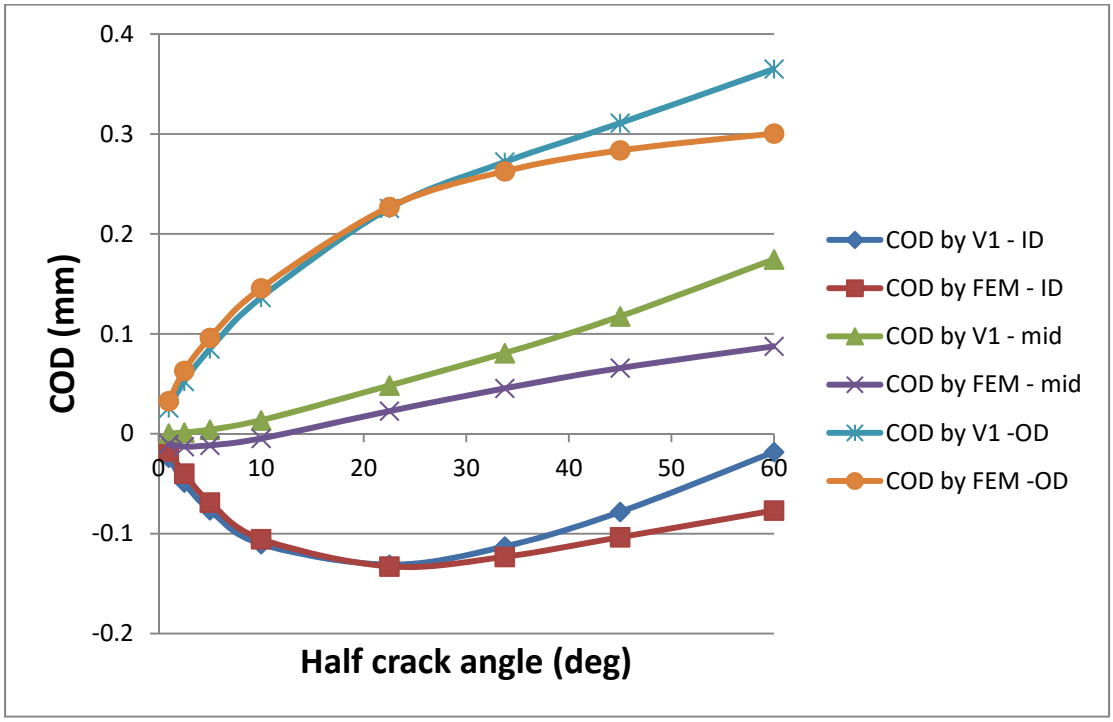

Figure 8 Validation of COD for Two-Part WRS field (R_m/t=10; WRS Mom. = 24626.3 N-mm)

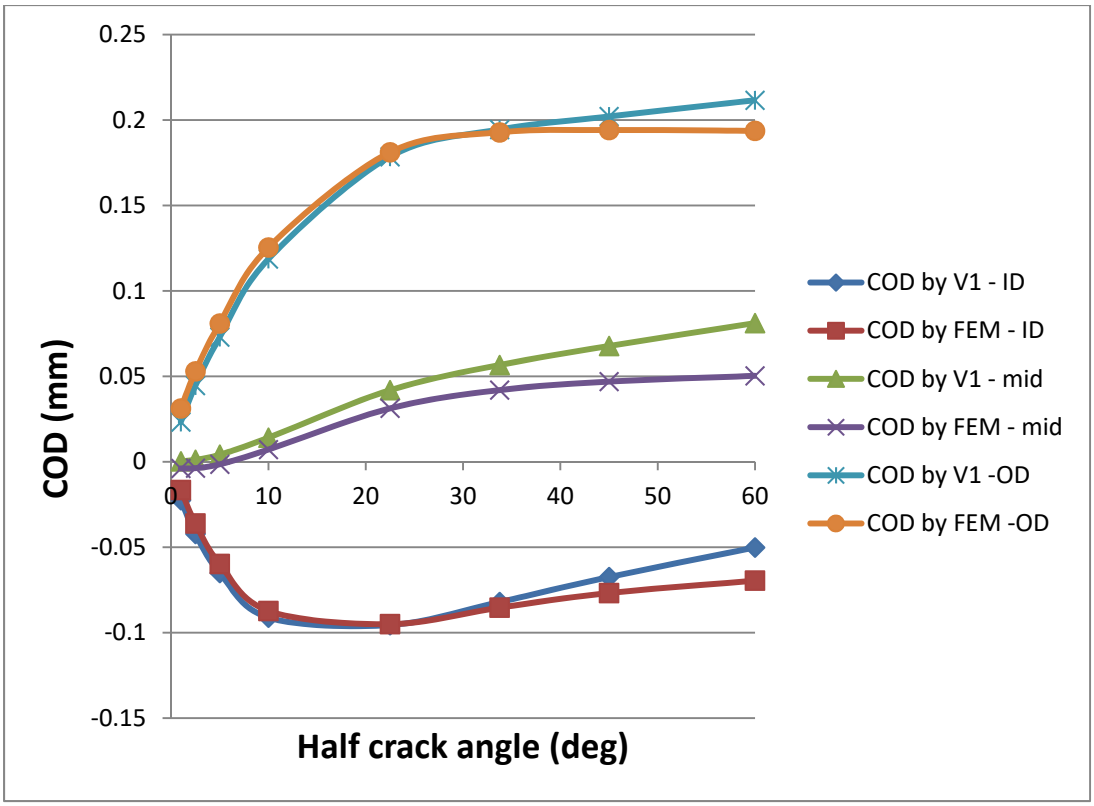

Figure 9 Validation of COD for One-Part WRS field (R_m/t=20; WRS Mom. = 6666 N-mm)

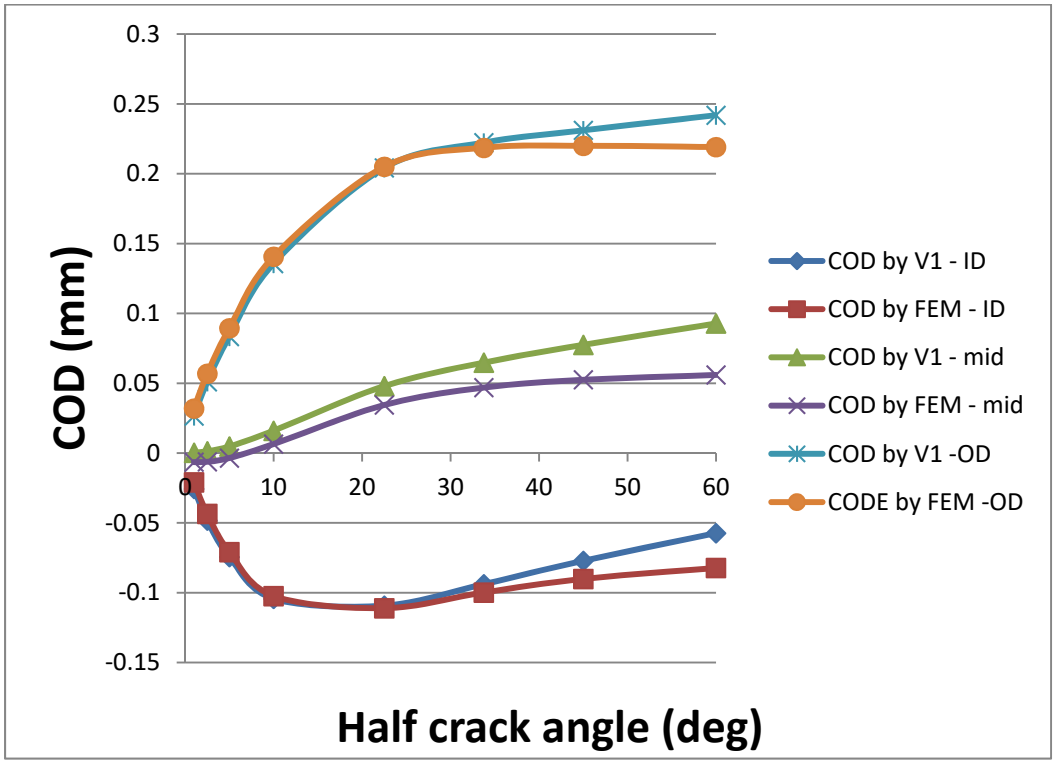

Figure 10 Validation of COD for Two-Part WRS field (R_m/t=20; WRS Mom. = 7622.4 N-mm)

6.1 Surge Line Validation Case

The actual surge geometry that is part of the NRC LBB round robin discussed in Appendix C was also considered. Figure 11 and Figure 12 show these comparisons for One-part and Two-part WRS distributions, respectively, that are described in Appendix C.

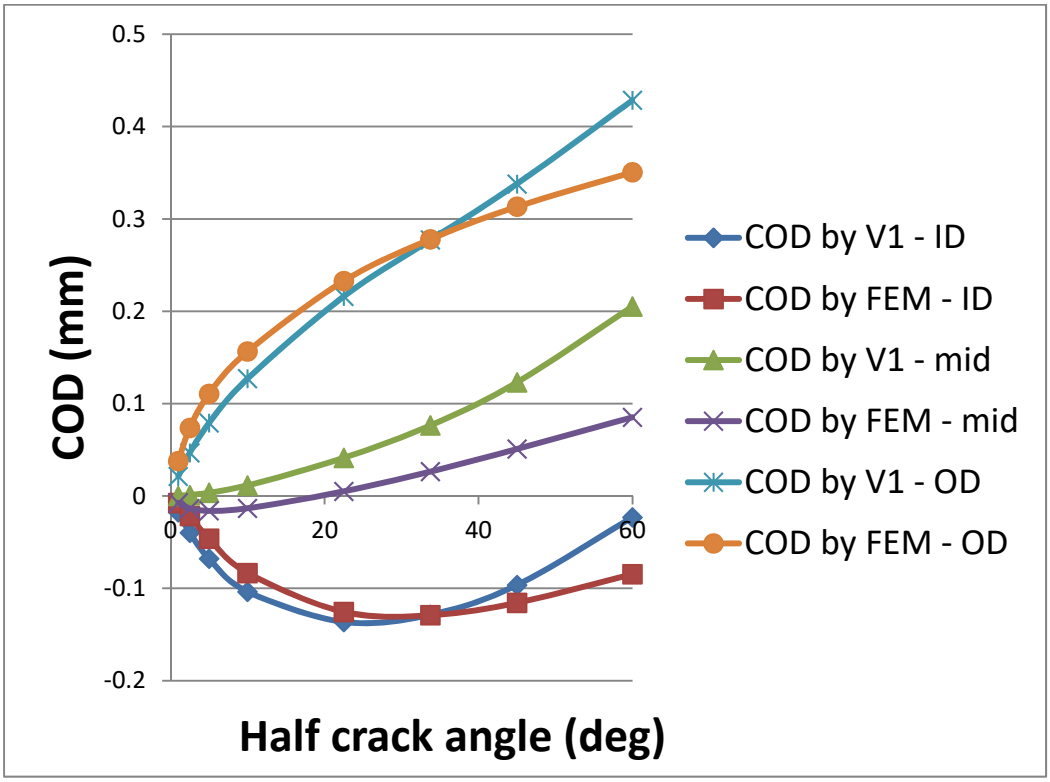

Figure 11 Validation of COD estimation for One-Part WRS field (R_m/t=4.5 LBB Round Robin) WRS Mom. = 81129.7 N-mm

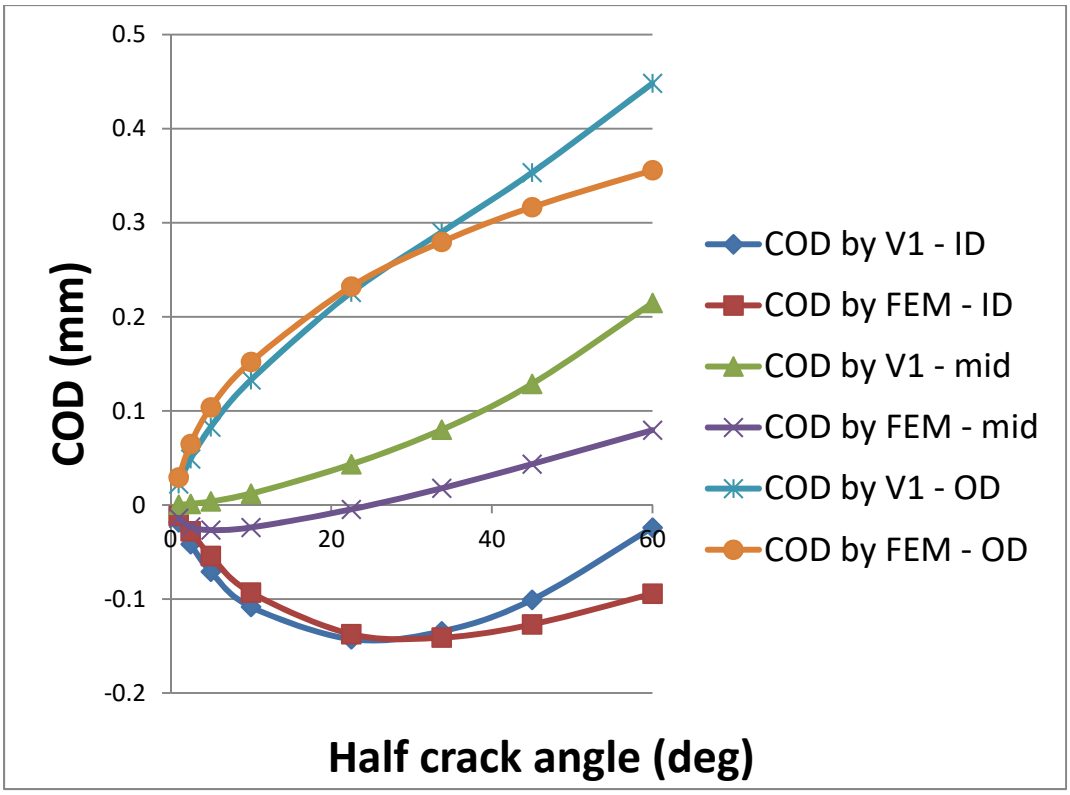

Figure 12 Validation of COD estimation for Two-Part WRS field (R_m/t=4.5 LBB Round Robin) WRS Mom. = 84838.1 N-mm

6.2 RPV Hot Leg Validation Case

Validation comparisons are also made to a reactor vessel hot leg nozzle geometry. This case is an analysis of a reactor pressure vessel nozzle weld that was evaluated using isotropic hardening; isotropic hardening tends to produce upper bound (in absolute value) WRS fields. The general WRS analysis procedure is summarized in the xLPR WRS final report (Brust, Benson, Broussard, 2016). For this case the actual WRS field was used to calculate the finite element based WRS COD results and then these were compared to the estimation scheme results. Details of the FE calculations are given in Appendix C.

The comparison between the finite element based COD analysis and the estimation scheme is shown in Figure 13. Again it is seen that the estimation scheme provides reasonable predictions of COD at the ID, mid-thickness, and OD despite the fact that this is a variable thickness nozzle and the estimation schemes were developed for constant thickness pipe.

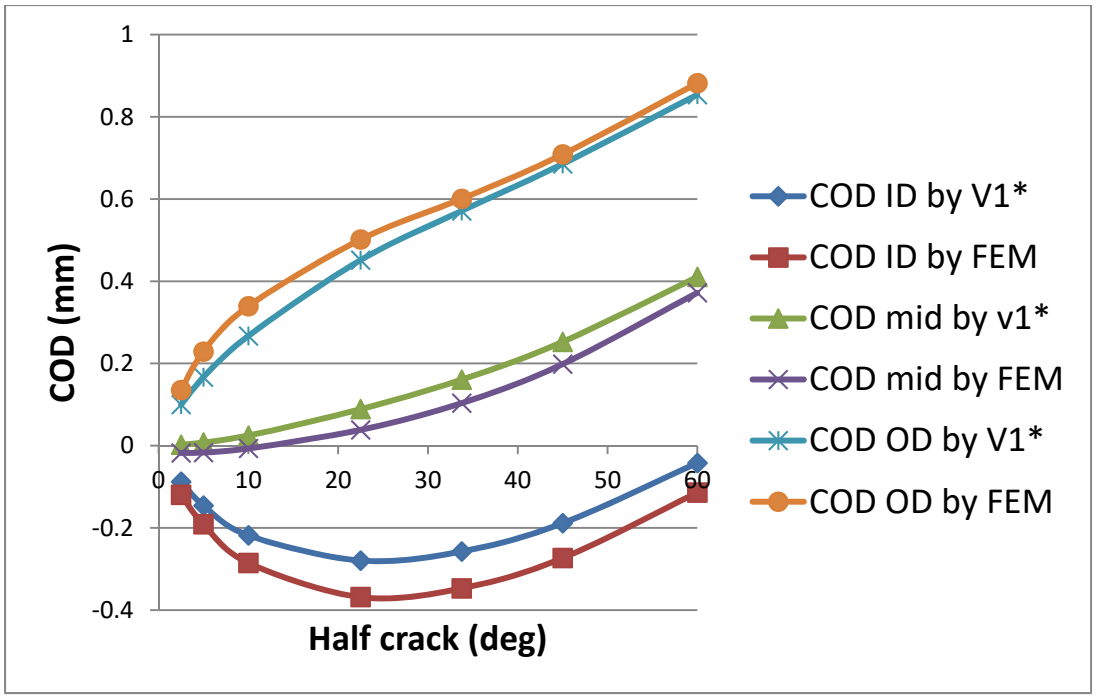

Figure 13 COD comparison for RPV nozzle

7. Summary and Discussion

Cracks in nuclear piping and nozzles often occur in and near welds, and weld residual stresses (WRS) can have a large effect on the COD values, even closing the crack under some circumstances. This report develops an engineering estimation scheme to predict the effect of WRS on COD predictions.

A simple estimation scheme, developed along the lines of classical COD estimation schemes based on influence functions developed from finite element solutions, is presented here. The estimation scheme is validated for different WRS fields for a wide range of half crack sizes, from 1-degree to 60-degrees, and a wide range of pipe geometries, ranging from 2 <= Rm/t < 20.

A methodology for estimating COD resulting from arbitrary WRS fields has been developed and the estimates have been benchmarked against FE. In general, the comparisons of the estimated COD to values determined by FE calculations are quite reasonable for an engineering estimation prediction method. The COD estimates generally work well for small crack sizes, a <= 45°, but deviate somewhat for smaller R_m/t values and for larger cracks where the COD contribution from service loads begin to dominate. Moreover, the mid wall COD estimates are less accurate for small R_m/t values.

Possible improvements to the estimation scheme are to:

- Modify the stress field used along the crack face to nonlinear fields. The linear case was included here and is shown to be relatively accurate. However, second and even third order effects can be included and will improve the accuracy of the method, particularly for larger crack sizes.

- Improve the description for midwall COD estimates, particularly for repair and inlay cases where there can be tensile stresses at the ID and OD and compressive stresses at the midwall. This case could be especially important as the midwall crack closure would be expected to affect COD, thus leak rate, but is not current considered in LBB evaluations. Currently, the linear WRS field used for this purpose goes through the mid thickness of the pipe (see for instance Figure 1). As seen in Figure 21 of Appendix C, the WRS fields used for validation often crossed the zero point at a value of x/t = 0.6 or greater where x is the distance from the ID. Using a nominal WRS field to produce the V_{1WRS} functions that crosses the zero line at other values might improve the mid wall WRS predictions. This would require development of some additional influence functions for these other cases.
- The results are developed for circumferential cracks in this report. However, the methods could be extended to axial cracks as well. For primary water stress corrosion cracking (PWSCC) concerns in pressurized water reactors, the hoop WRS fields are usually higher than axial stresses. This often means that a leak from an axial crack can occur long before a circumferential crack will leak. However, if the WRS fields pinch the axial cracks such cracks may not leak as much due to pinching of the crack faces. Therefore, it may be useful to develop the engineering estimation scheme for axial cracks as well. This might lead to improvements in the xLPR code as well as often xLPR predicts axial crack leakage first and corresponding detection. This will affect the risk.
- Examine the possible effects of plasticity on the WRS based COD values. This may only be important for small Rm/t values and small cracks – but it should be investigated.

8. References

ASME, (1986), "Evaluation of Flaws in Austenitic Steel Piping," Technical basis document for ASME IWB-3640 analysis procedure, prepared by Section XI Task Group for Piping Flaw Evaluation, EPRI Report NP-4690-SR, April 1986.

Brust, F. W. (1987), "Approximate Methods for Fracture Analysis of Through-Wall Cracked Pipes", Topical Report, Battelle Columbus Laboratories, NUREG/CR-4853.

Brust, et al. (1995), "Assessment of Short Through-Wall Circumferential Cracks in Pipes", NUREG/CR-6235, BMI-2179.

Brust, F. W., Punch, E., Twombly, E., Kalyanam, S., Kennedy, J., Hattery, G., Mach, J., Webb, J., Dodds, R. H., Nicklas, J., Gohar, B., Hudak, D., Chalker, A. (2016), "Adoption of High Performance Computational (HPC) Modeling Software for Widespread use in the Manufacture of Welded Structures", Final Report on Grant Award No. DE-SC0009494, DOE SBIR Program Office, December (https://www.osti.gov/biblio/1349722).

Brust, F. W., Benson, M., Broussard, J., Cox, A., Kurth, R., and Sallaberry, S. (2016), "Technical Basis Document, Welding Residual Stress Modeling Development", final summary for xLPR code documentation, October.

Cherepanov, G. P. (1967), The propagation of cracks in a continuous medium, Journal of Applied Mathematics and Mechanics, 31(3), pp. 503–512.

Hutchinson, J. W. (1968), "Singular behaviour at the end of a tensile crack in a hardening material" (PDF), *Journal of the Mechanics and Physics of Solids*, **16** (1): 13–31.

Ilyushin, A. A. (1946), "The theory of Small Elastic-Plastic Deformations", Prikadnaia Matematika I Mekhanika, PMM, Vol. 10, pp. 347-356.

Kumar, V., German, M., and Shih, C. F. (1981), "An Engineering Approach for Elastic-Plastic Fracture Analysis," EPRI Report No. NP-1931, July 1981.

Kumar, V., German, M., Wilkening, Andrews, W., deLorenzi, H., and Mowbray, D. (1984) "Advances in Elastic-Plastic Analysis," EPRI Final Report NP-3607, August 1984.

Kumar, V. A. G. M., & German, M. D. (1988). "Elastic-plastic fracture analysis of through-wall and surface flaws in cylinders", (No. EPRI-NP-5596). General Electric Co., Schenectady, NY (USA). Corporate Research and Development Center.

Milne, I, Ainsworth, R. A., Dowling, A. R., and Stewart, A. T. (1986), "Assessment of the Integrity of Structures Containing Defects, CEGB Report R/H/R6 - Revision 3," 1986.

Olson, R. (2016), "A Simple Approach for Including Weld Residual Stresses in the Calculation of Pipe Circumferential Through-Wall Crack Opening Displacements", Proc. ASME PVP, PVP2016-63169, Vancouver, BC, July 17-21.

Rahman, S., and Brust, F. W. (1992), “Elastic-Plastic Fracture of Circumferential Through-Wall Cracked Pipe Welds Subject to Bending”, ASME Journal of Pressure Vessel Technology, Vol. 114, pp 410-416, March.

Rice, J. R. (1968), “A Path Independent Integral and the Approximate Analysis of Strain Concentration by Notches and Cracks”, Journal of Applied Mechanics, 35, pp. 379–386.

Rice, J. R., Rosengren, G. F. (1968), "Plane strain deformation near a crack tip in a power-law hardening material", *Journal of the Mechanics and Physics of Solids*, **16** (1): 1–12.

Wilkowski, G. M., et al. (1992), "Short Cracks in Piping and Piping Welds," NUREG/CR-4599, BMI-2173, Vol. 1, No. 2, prepared by Battelle Memorial Institute, April.

Young, B. A., Olson, R., & Kerr, M. (2012), “Advances in COD Modeling: Circumferential Through-Wall Cracks”, ASME International, PVP 2012, PVP2012-78181, Toronto, ON, Canada, July.

Young, B. A., Olson, R., & Scott, P. M. (2013), “Advances in COD Modeling – Multiple Loading Modes: Concurrent Axial and Crack Face Pressure with a Subsequent Applied Bending Moment,” Structural Mechanics in Reactor Technology (SMiRT) 22, San Francisco, CA, August 2013.

Appendix A

Short Summary of Classical J-Theory and Estimation Schemes for NRC Use

J-Tearing theory arose out of the "HRR" mathematically based asymptotic field solutions developed independently by Rice and Rosengren (1968) and Hutchinson (1968). The asymptotic solutions assume elastic-plastic behavior characterized by a Ramberg-Osgood material law although the concepts apply equally to flow theory as long as unloading does not occur. The J-Integral (or 'J') represents the strength of this asymptotic field and therefore is assumed to characterize the fracture response of elastic and power law hardening materials. This asymptotic based fracture theory is similar to how the stress intensity factor represents the strength of the elastic field and therefore is the elastic fracture parameter.
One convenient feature, shown by Rice (1968) and earlier by Cherepanov (1967), is that the J-integral is path independent when calculated along a path that encircles the crack tip as long a proportional loading persists. This permits calculation of the fracture parameter, J, at locations far from the crack tip away from potential numerical solution errors inherent in finite element solutions for instance.

During loading when J reaches the experimentally determined J_R initiation value the crack begins to grow. Crack growth is then predicted until the dJ/da driving force exceeds the resistance or dJ_R/da, where 'a' is crack size. Despite the fact that proportional loading is violated once crack growth occurs the theory has been shown to provide good engineering predictions of crack growth and instability over the years (see the series of NRC funded work over the years as for instance in Wilkowski (1992) and many references cited therein).

J-estimation scheme methods for elastic-plastic fracture have been developed based on J-Tearing theory over the years in many different ways. The convenient development of estimation schemes is based on the theorems of Ilyushin (1946) who proved that the field solutions to the boundary value problem involving a monotonically increasing load or displacement-type parameter is proportional for a power law material. This permits development of the estimation schemes for all fracture-based field parameters including J, crack opening displacements, far field displacements, and other parameters. This process is summarized in a number of references (Kumar (1982), Brust, (1987), Rahman and Brust (1992) and many references cited therein) where estimation schemes are developed and summarized using a variety of methods including numerical and equivalence methods.

Detailed overviews of the various elastic-plastic fracture estimation methods were provided in Brust et al. (1995), including short overviews of the model development of each of these. These major J-estimation methods include:

- Numerically based methods (Kumar (1981, 1988), Brust et al (1995), Young et al (2012)). This involved development of a series of numerical solutions and influence function tables which are interpolated between to estimate the various parameters including J and COD.
- Equivalence based methods (Brust (1987)). These methods model the crack using an equivalent geometrical shape meant to mimic the reduction in stiffness caused by the crack and lead to closed form solutions for J and COD. Such closed form solutions are very convenient for probabilistic fracture codes such as xLPR because of solution speed. While the estimate of J using these methods is quite good for stability predictions, the estimate of COD is rather poor because of the reduced thickness analogy.

- Z-Factor approach of ASME Section XI IBB-3640 (ASME, 1986). This method applies a correction to the limit load solutions which depends on the material ductility to predict crack instability. COD predictions are not possible with this method.
- Reference stress methods (Milne, 1986). These methods are popular in Europe for instability predictions but estimates of COD are not adequate.

From this discussion it is apparent that numerical estimation methods are most accurate for COD predictions and it is the method chosen here to predict the effect of WRS on COD.

Appendix B

WRS Moment Equation for Linear WRS Field

Taking a sector of pipe with unit arc length on mean radius $r_m = (r_o + r_i)/2$, specify that the axial stress is σ on the outer diameter and –σ on inner, separated by pipe thickness *t*, where r_o and r_i and r_m are outer, inner, and mean radius, respectively). The linearly varying axial stress at any radius r becomes

$$\sigma_z = \frac{\sigma(r - r_i)}{t} - \frac{\sigma(r_o - r)}{t}$$

By integrating the increment of axial force $dF = \sigma_z.(r/r_m)\, dr$, the force per unit arc length on r_m is

$$F = \int \sigma_z . \left(\frac{r}{r_m}\right) . dr$$

$$F = \frac{\sigma\left[2\frac{\left(r_o^3 - r_i^3\right)}{3} - r_m.\left(r_o^2 - r_i^2\right)\right]}{t.r_m}$$

$$F = {\sigma t}/{(6\varphi)}$$

where $\varphi = R_m/t$.

Hence the linear stress distribution has an axial disequilibrium stress $\sigma_{dis} = F/t = \sigma/(6\varphi)$.

The equilibrated stress distribution is $\sigma_{eq} = \sigma_z - \sigma_{dis}$ and the associated moment about pipe center is

$$M = \int \sigma_{eq} . r . \left({r}/{r_m}\right) dr$$

After considerable algebraic manipulation, it can be shown that this integral reduces to the expression

$$\frac{M = \frac{\sigma t^2}{3} - \frac{\sigma t^2}{18}\left(r_o^2 + r_o.r_i + r_i^2\right)}{rm^2}$$

$$= \frac{\sigma t^2}{6}\left[1 - {1}/{12\varphi^2}\right]$$

For very thin pipes, disequilibrium stress and moment become 0 and $\sigma t^2/6$, respectively (i.e. planar plate stress).

Appendix C
Finite Element Calculations for Influence Function Determinations

Finite element-based predictions of the WRS effect on COD are typically performed in the following manner. An axis-symmetric weld residual stress analysis is performed. The WRS field is then rotated into a full three-dimensional field but the residual stresses are axis symmetric. Sometimes these stresses are mapped to a coarse two-dimensional axis-symmetric solution first before using a rotational transformation to produce a coarse three-dimensional solution. This WRS field is then mapped onto a full three-dimensional crack mesh with spider type mesh refinement along the crack. The mapping procedure within ABAQUS performs very well for this purpose. The crack is then introduced in this model assuming elastic behavior and the effect of the WRS field on the COD is then determined. Additional fracture parameters such as the stress intensity factor can also be determined but here, we are only interested in the WRS on COD effect. Alternatively, the WRS field can be introduced into the crack mesh by introducing a thermal gradient field into the crack mesh before introducing the crack. A simple iterative procedure has been developed (not discussed here) that permits determination of the thermal field that will produce the desired WRS field. Both of these example methods are illustrated later.

The above process produces a weld residual stress field of interest and our goal is to predict, using the estimation scheme developed here, the COD that develops from this WRS field. An example of the generic solution mesh used for the $R_m/t=5$ case for development of the influence functions is shown in Figure 14. This is a quarter symmetric model with the crack placed on the axial (Y-direction) symmetry plane. Appropriate boundary conditions were applied on the symmetry planes. This is for the case of $R_m/t=5$ with a 10-degree crack. A linear 'unit' moment of +- 100 MPa was applied in an axis-symmetric fashion along the crack.

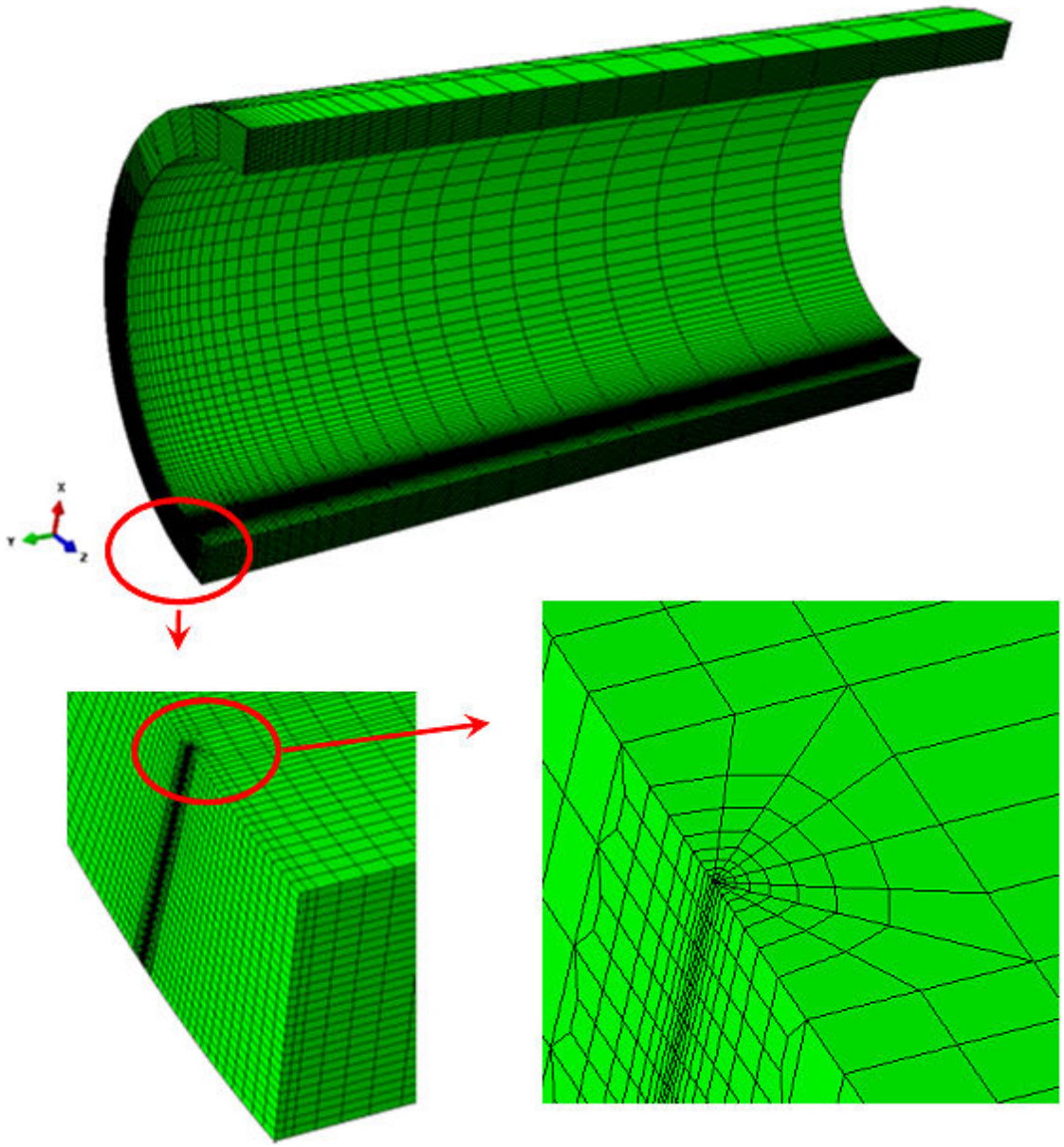

Figure 14 Generic mesh used to develop V_{1WRS} functions (R_m/t=5, 10-degree crack)

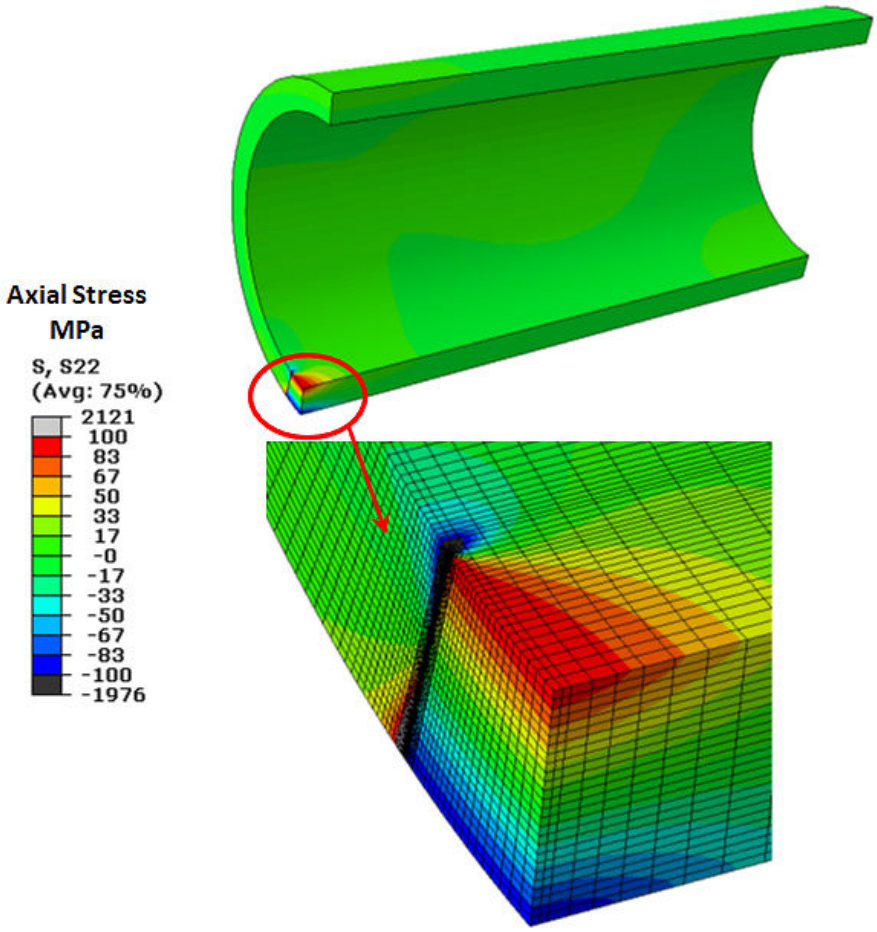

Figure 15 Generic WRS field (+- 100 MPa) to develop V_{1WRS} functions (R_m/t=5, 10-degree crack)

This unit moment was applied with ABAQUS using a DLOAD subroutine developed by the authors. The stresses were slightly different from +-100 MPa to ensure that an equilibrium stress field was applied using the dis-equilibrium stress correction shown in Equation (3). An example of this is shown in Figure ***15*** where the nominal +- 100 MPa stress field on the crack is illustrated. Note that the stresses at the crack tip are large due to the singularity caused by the crack in this elastic solution.

Validation comparisons of the WRS COD estimation procedure were made for a large number of different example cases discussed in the main body of the report. Each case had different size crack and a different WRS field. The WRS field for this geometry was applied by introducing a thermal field on the cracked finite element mesh. A WRS field produced in this manner provides an accurate assessment of WRS fields.

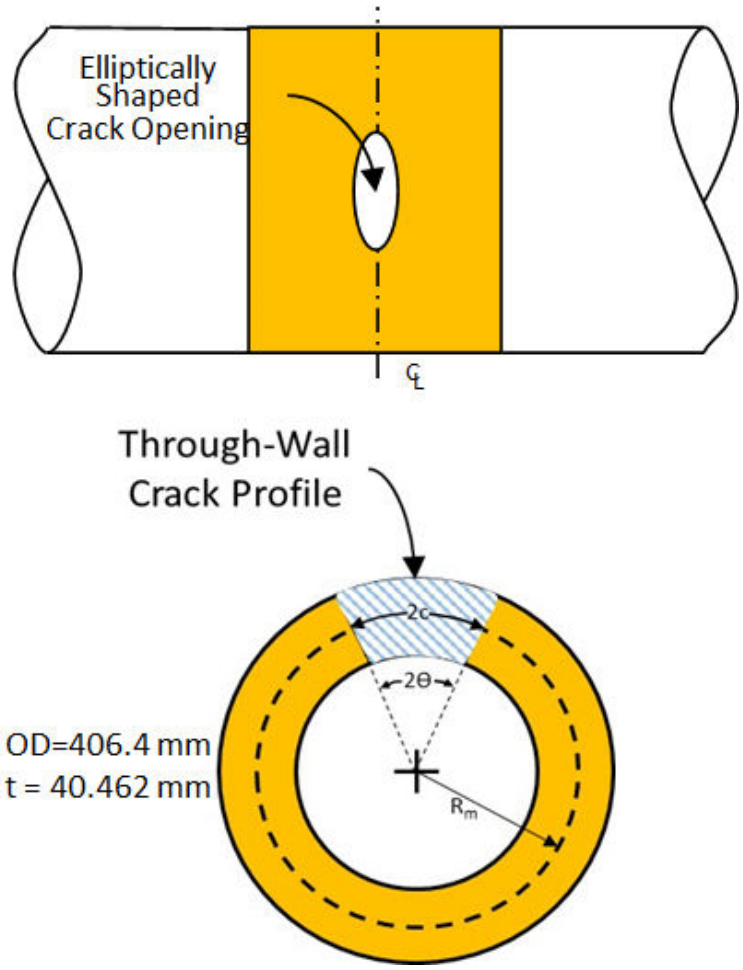

Figure 16 NRC LBB round robin problem definition (R_m/t=4.5)

A surge type geometry was used by the US NRC in an LBB round robin problem recently as illustrated in Figure 16. A computational weld analysis was performed for this problem prior to introduction of a crack. The original WRS analysis results are shown in Figure 17 with the stress plotted through the thickness in Figure 18.

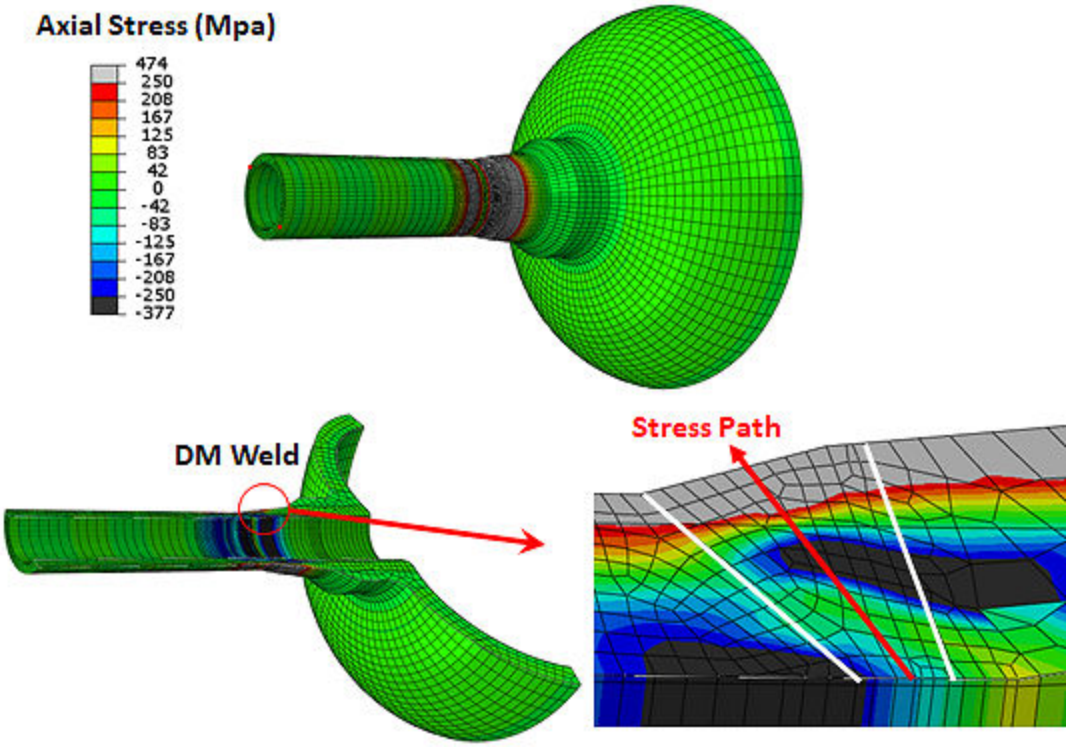

Figure 17 Original WRS field for NRC LBB round robin problem

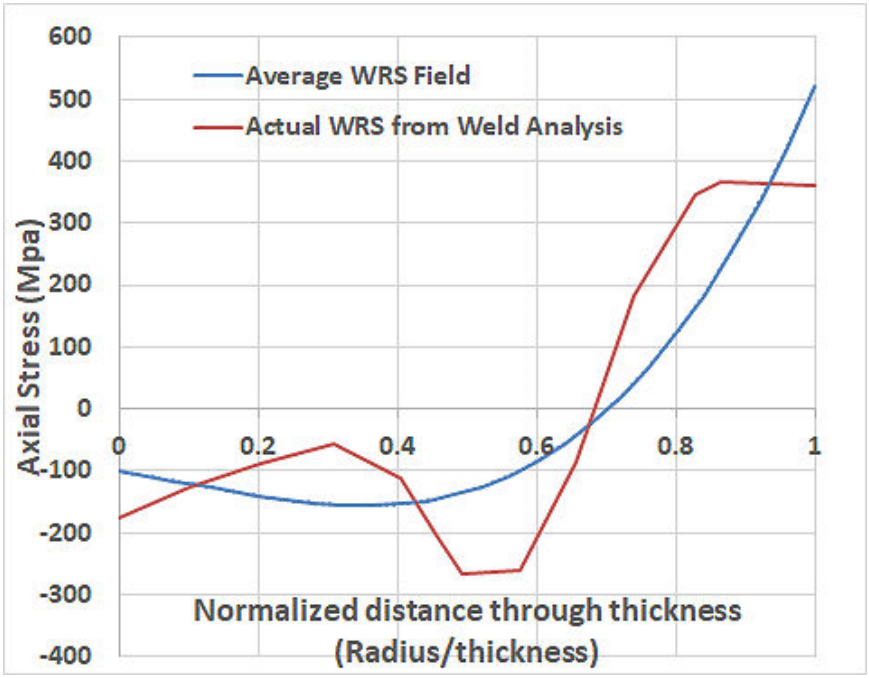

Figure 18 WRS field plotted through thickness along red line in Figure 17 ($R_m/t=4.5$)

The FE model of the surge line is shown in Figure 17 and the stresses were obtained from a bead-by-beak deposition weld analysis on an axis-symmetric surge nozzle geometry. This WRS was then mapped onto a coarse axis-symmetric WRS field and then this was rotated to a full three dimensional mesh as seen in Figure 17. The plot of actual WRS field through the thickness along the red "Stress Path" line of Figure ***17*** is given by the 'red' curve in Figure 18 and the 'blue' curve is the third order polynomial fit of the WRS field that was used in the NRC LBB round robin problem. Both the 'red' and the 'blue' WRS fields were used for a variety of pipe sizes and crack sizes to validate the accuracy of the WRS COD procedure developed here. These were referred to as 'One Part' and 'Two Part' WRS fields. The terms 'one part' and 'two part' are used because, for the more complicated WRS field at bottom of Figure 19, the use of two thermal fields are required to obtain the WRS field while for the simpler WRS field at the top of Figure 19 one thermal field through the thickness is all that is required.

The validation analyses shown in Section 6 were performed by applying a thermal field as seen in Figure ***19***. In Figure 19 the bottom plot represents the actual WRS field produced from the weld analysis and corresponds to the actual WRS field shown in Figure 17 and Figure 18. This is referred to at the 'two part' WRS field. The 'black' curve represents the WRS field obtained by applying an appropriate thermal gradient to the model. A simple procedure has been developed to iterate on the temperatures until the WRS field becomes close to the actual WRS field. It usually takes about 4 to 6 iterations until the temperature field from the thermal gradient solutions matches the actual WRS field. The upper curves in Figure 19 show another thermal field developed to model the WRS field of the average curve in Figure 18 and this stress field was used for the LBB round robin problem. The above stress fields are for the geometry for straight pipe (Figure 16) rather than the nozzle geometry shown in Figure 17.

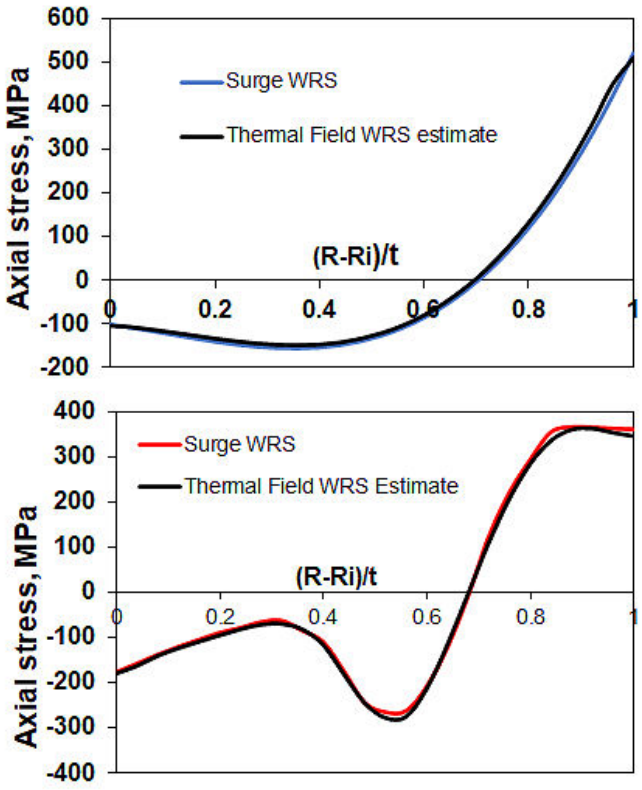

Figure 19 WRS field plotted through thickness for thermal field and actual WRS (R_m/t=4.5) The upper plot is a third order polynomial representation of the data from the lower plot and can be modeled well with a One-Part thermal field.

This same temperature field was used for the validation cases shown below for the various pipe sizes (R_m/t values of 2, 5, 10, and 20). The WRS field varies for each R_m/t case when this temperature field is applied. The same thermal field is applied in each case but, because of the different geometries, differences in the WRS fields result – see Figure 21. Therefore, the validations are performed for many different WRS fields applied for different cracked pipes and represents a robust set of validation cases. Both WRS fields of Figure 19 are considered for the WRS COD validation cases.

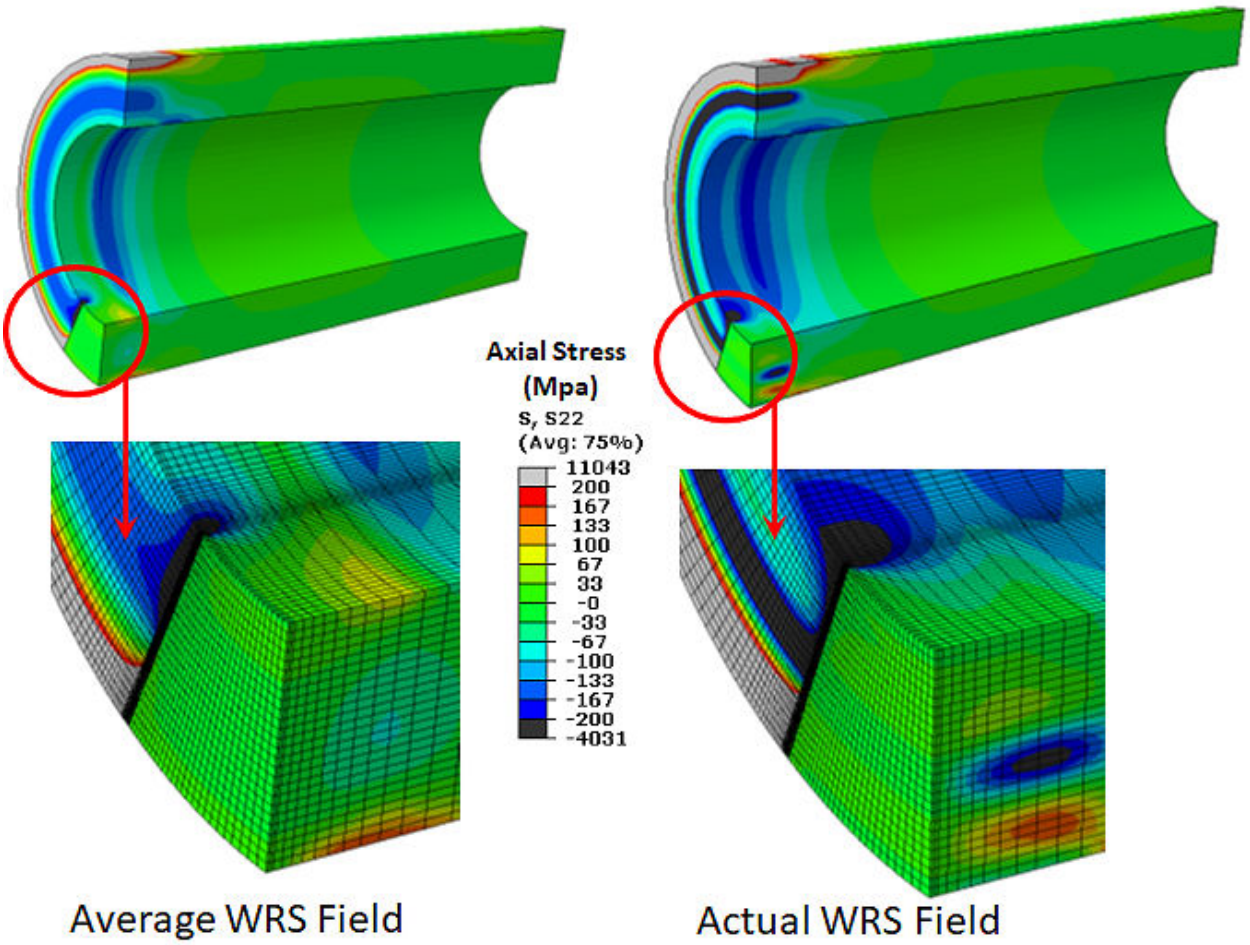

Figure 20 WRS field plotted through thickness for thermal field (R_m/t=2, θ=22.5-degree)

An example validation case mesh is shown in Figure 20 for the R_m/t = 2 case and crack 22.5-degree. Since the same temperature field produced by the R_m/t=4.5 surge mesh is used by these validation cases, the WRS field differs from that shown in Figure 19 for each pipe geometry. Figure 21 illustrates the WRS fields produced for the validation cases for R_m/t = 2, 4.5, and 20 where it is seen that they are different. The first step in predicting the COD using the present estimation scheme is to determine the moments for the WRS distributions (like Figure 21) for the geometry of interest using the procedure illustrated for

Table **5** above. Then the estimate of COD is made with the estimation scheme and compared to the full FEA solutions. This is shown below.

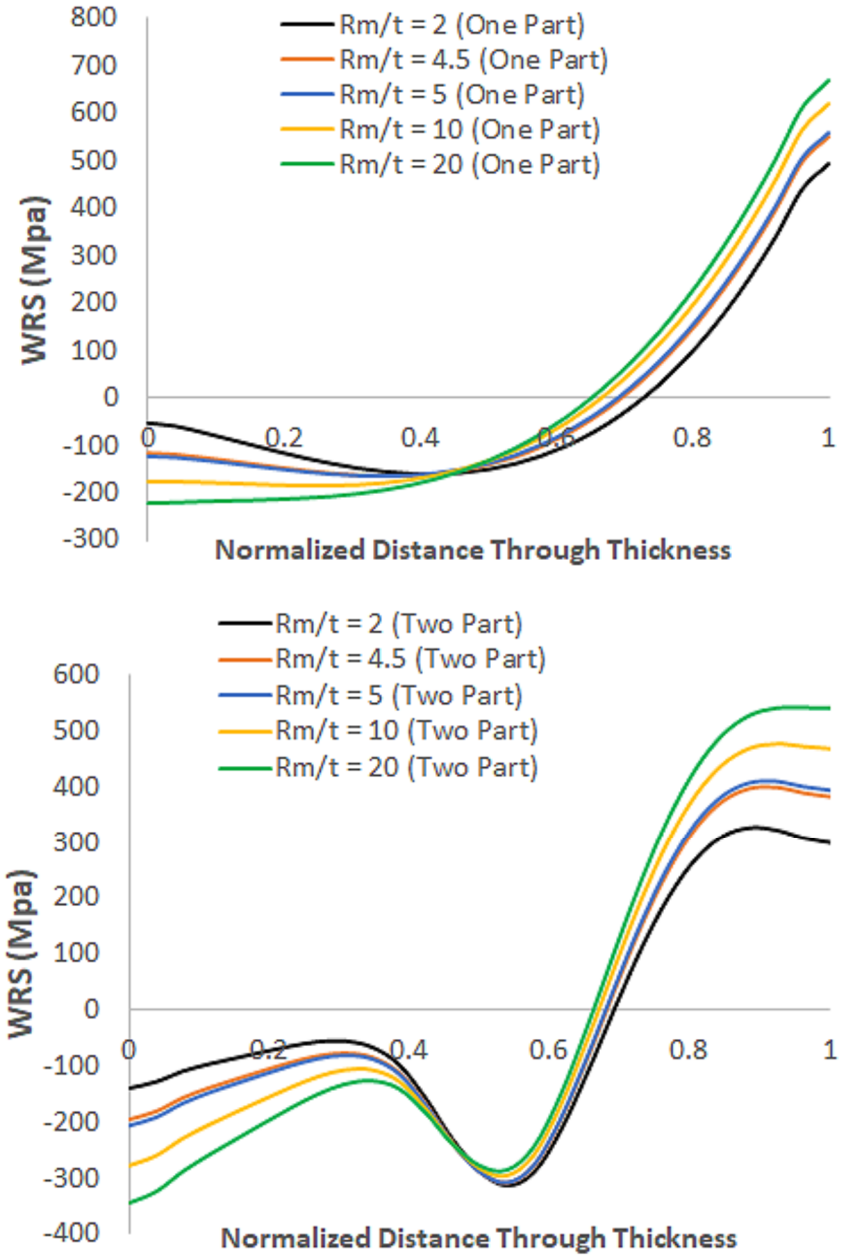

Figure 21 Thermal WRS field plotted through thickness for thermal field (R_m/t=2, 4.5, 20)

RPV Nozzle Validation Case

For the RPV validation case the actual WRS field that was determined from FE calculations was used. The WRS field was developed by modeling the bead-by-bead deposition on an axis-symmetric model.

The axis-symmetric field variables were then mapped to a coarser two-dimensional axis-symmetric mesh and then rotated into a 3D model using the appropriate ABAQUS procedures. This WRS field was then mapped onto each crack mesh and the crack was opened up to obtain the finite element-based COD values caused by the WRS field. These are then compared to the estimation scheme for various crack sizes.

The finite element mesh for this crack assessment is illustrated in Figure 22 and a plot of the WRS field before and after introduction of the crack is shown in Figure 23 where the closure of the crack can be seen. The crack contact that would occur when crack faces partially close (Figure 23) is not included in these calculations which is why negative crack opening displacements are possible with closing WRS fields. This geometry had an R_m/t value of 6.02. The through thickness WRS field at the weld centerline is plotted in Figure 24.

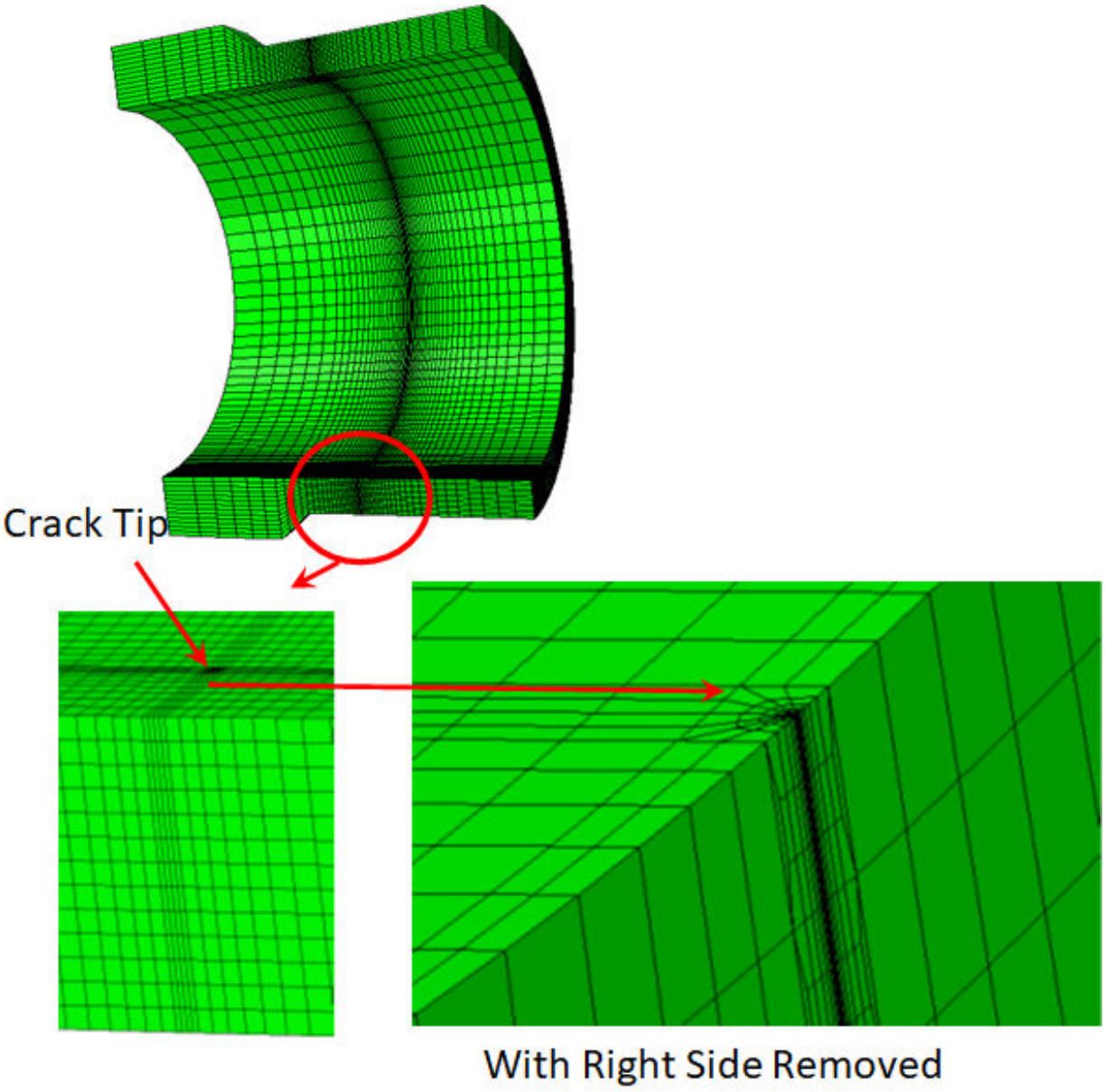

Figure 22 Crack FEA mesh for RPV with 15% repair 5-degree crack angle

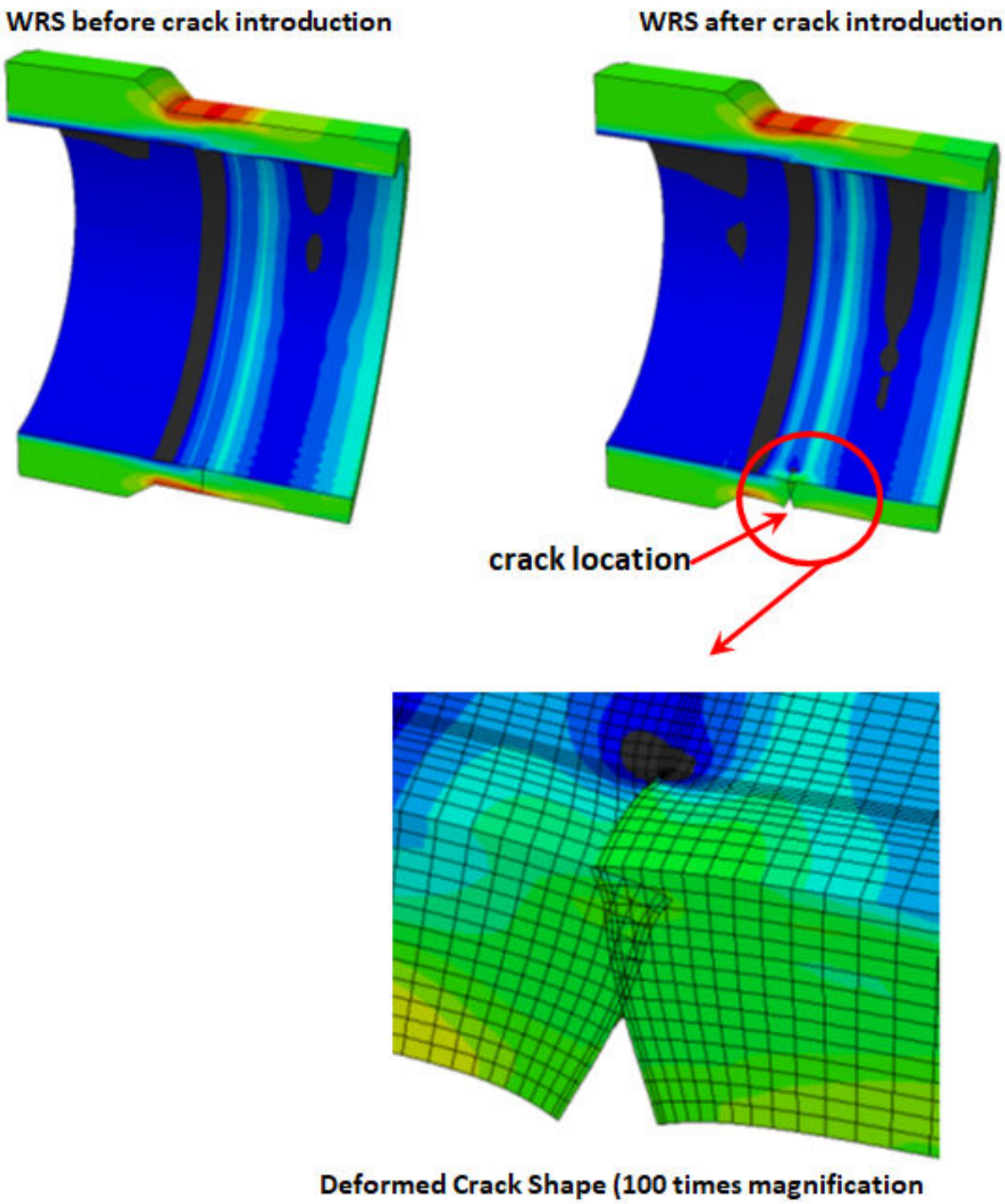

Figure 23 WRS field before/after crack for RPV with 15% repair 5-degree crack angle

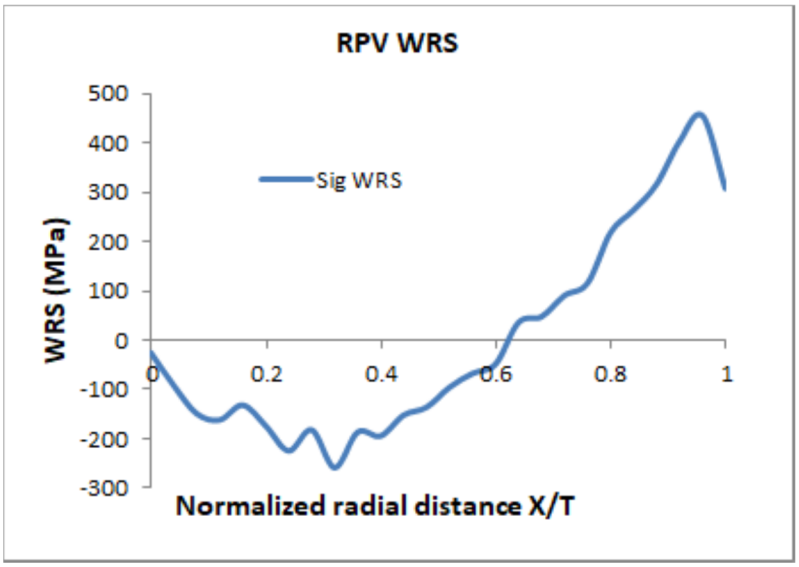

Figure 24 WRS field plotted through thickness at weld center for RPV